Hyperloop or Bust

Kenneth Decker,[*] Andi Peng,[†] Colin Summers[‡] Golda Nguyen,[§]
Andrew Oberlander,[¶] Gazi Sakib,[‖] Nathan Sharifrazi,[**] Jeffrey Chin,[††]
Justin Gray,[‡‡] Christopher Heath,[‡‡] Kenneth Moore,[‡‡]
Robert Falck,[‡‡]
NASA Glenn Research Center, Cleveland, OH

[*]Aerospace Engineer, University of Arizona
[†]Computer Science, Politcal Science, Yale University
[‡]Chemical Engineer, Computer Engineer, University of Washington-Seattle
[§]Mechanical Engineer, Georgia Institute of Technology
[¶]Mechanical Engineer, Brown University
[‖]Physics, Mechanical Engineer, Stony Brook University
[**]Aerospace Engineer, Mechanical Engineer, University of California-Irvine
[††]Aerospace Engineer, Propulsion Systems Analysis Branch, Mail Stop 5-10, AIAA Member
[‡‡]Aerospace Engineer, MDAO Branch,Mail Stop 5-10, AIAA Member

Contents

I. Editing Notes

II. Introduction

[c1]

Background of Hyperloop -DOT Takeaways and Key Research Questions
-Shortcomings of short-haul aviation
-Shortcomings of high speed rail project / driving

History of Hyperloop Historical Precedents -Musks Hyperloop Alpha - Current Players/Pursuants/Involvement
–Perhaps brief snippet about Hyperloop student competition
–Hyperloop One
-Jeff and Justins Conceptual Design Paper

How Hyperloop solves problem -Cleaner, faster, cheaper, bitch!
-High level technological overview

Layout about what this paper addresses -Full system model in OpenMDAO
–Technological feasibility
–Economic feasibility
-Trade Studies
-Conclusions

III. Hyperloop System Model Overview

Hyperloop System Model Overview

The Hyperloop full-system model is decomposed into two main subsystems-the passenger pod and tube. At the top level, analyses was performed integrating the pod and tube systems with a ticket cost module and sample mission module. Tree diagrams for the passenger pod and tube systems can seen below:

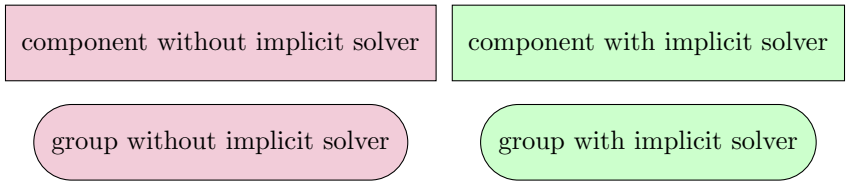

Figure 1: Tree view and XDSM diagram key

Further sub-systems were broken down within the pod and tube components, and are detailed below. Full documentation can be found in the following sections of the Appendix: [c2]

A. Top Level Component Descriptions

1. Pod

The construction of the tube is driven by the configuration of the pod. Consequently, the system model is constructed such that the pod design configuration is analyzed first. The pod group contains all subsystems onboard the pod. The pod takes in user variables set by the user and feeds them into drag, cycle, drivetrain,

[c1] *Colin*: who is writing introduction?
[c2] *Colin*: need to actually reference the Appendix for detailed info

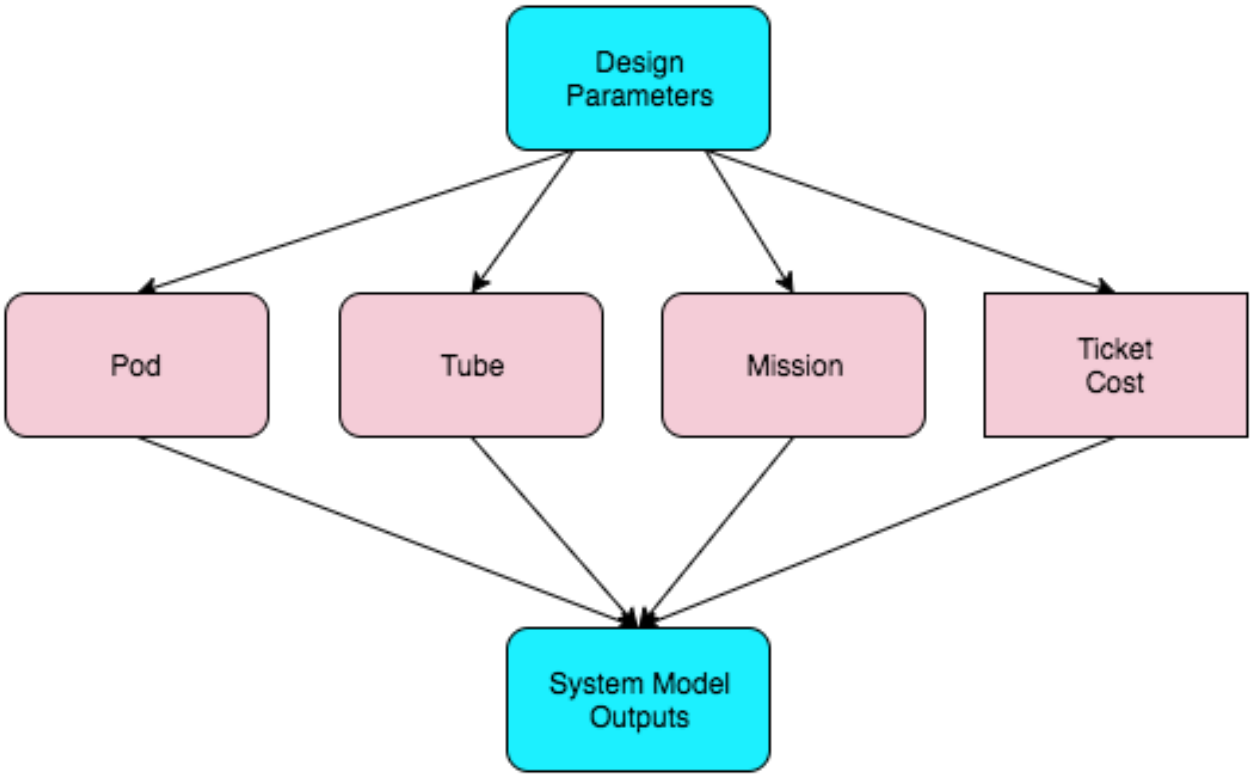

Figure 2: Hierarchial tree digram showing overall model structure

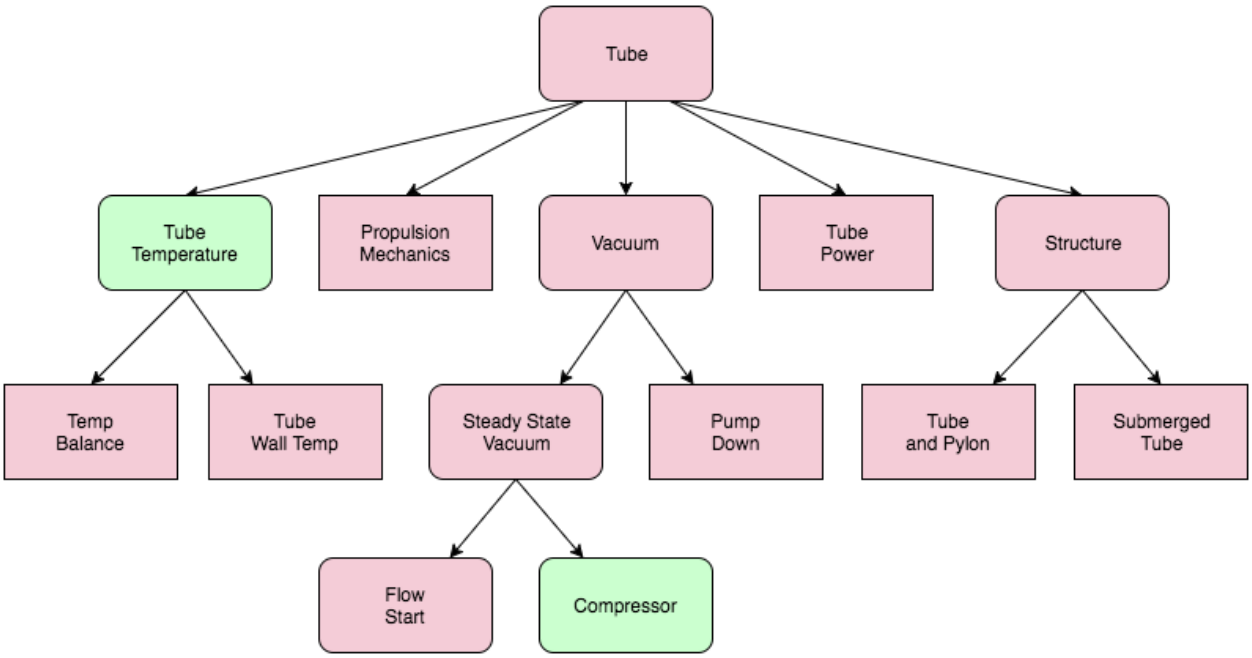

Figure 3: Hierarchial tree digram showing structure of TubeGroup

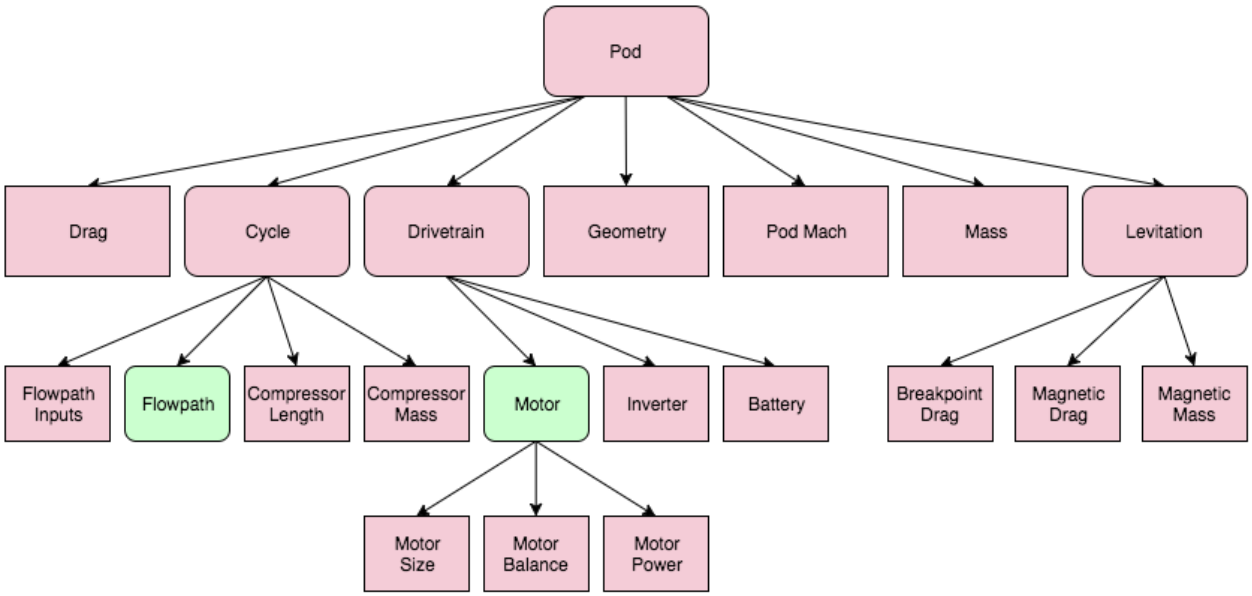

Figure 4: Hierarchial tree digram showing structure of PodGroup

geometry, mass, and levitation subsystems. When executed, the pod group outputs all relevant information about the pod configuration and design needed to evaluate system performance [c3].

2. Tube

Once the pod group determines the design configuration of the pod, the tube group is able to analyze the tube design. The tube group contains subsystem analyses for the vacuum pumps, the electromagnetic propulsion system, thermal management, and tube structure. Once the major aspects of the design of the tube are evaluated, results for both pod and tube design can be fed into mission and cost analyses to evaluate overall system performance requirements and their resulting costs[c1].

3. Mission

It is necessary to obtain a reasonable estimation of the mission performance requirements in order to carry out system level trade studies. It is important to note that the exact mission route is dependent on the topography of the land between the two notional endpoints. Currently, it is beyond the scope of the model to account for the effect that varying topology will have on the pods trajectory. For simplicity, the model is assumed to travel in a straight, flat line between the departure and arrival locations, in this case the LAX and SFO airports. The mission velocity profile contains three phases: acceleration, coasting with periodic boosting sections, and deceleration[c2c3]. Figure 5 shows what a possible velocity profile would look like using this mission analysis model. The initial acceleration is modeled as a constant linear acceleration of 1g from rest to top speed. Previous analyses have modeled the start up as an incremental acceleration, as is shown in fig. 5, due to allow for more maneuverability and to avoid sustaining potentially uncomfortable g forces for to prolonged periods of time.[1] This produces a negligible difference in energy consumption from the model used in this analysis. The second phase of travel consists of a coasting pod with periodic boosting sections. In this phase, the pod begins at top speed and is allowed to coast until it reaches some minimum speed set by the user. Then, the will enter an electromagnetic boosting section which will accelerate the pod at 1g back to the desired top speed. For straight and level travel, the acceleration of the pod is given by the equation

$$\frac{\mathrm{d}v}{\mathrm{d}t} = f(v) = \frac{1}{m}(F_{thrust} - \frac{1}{2}C_D\rho V^2 S - D_{mag}) \tag{1}$$

[c3] *Colin*: seems like this could be 1-2 sentence
[c1] *Colin*: seems like this could be 1-2 sentence
[c2] *Colin*: shorten up text
[c3] *Colin*: how large do our figures need to be?

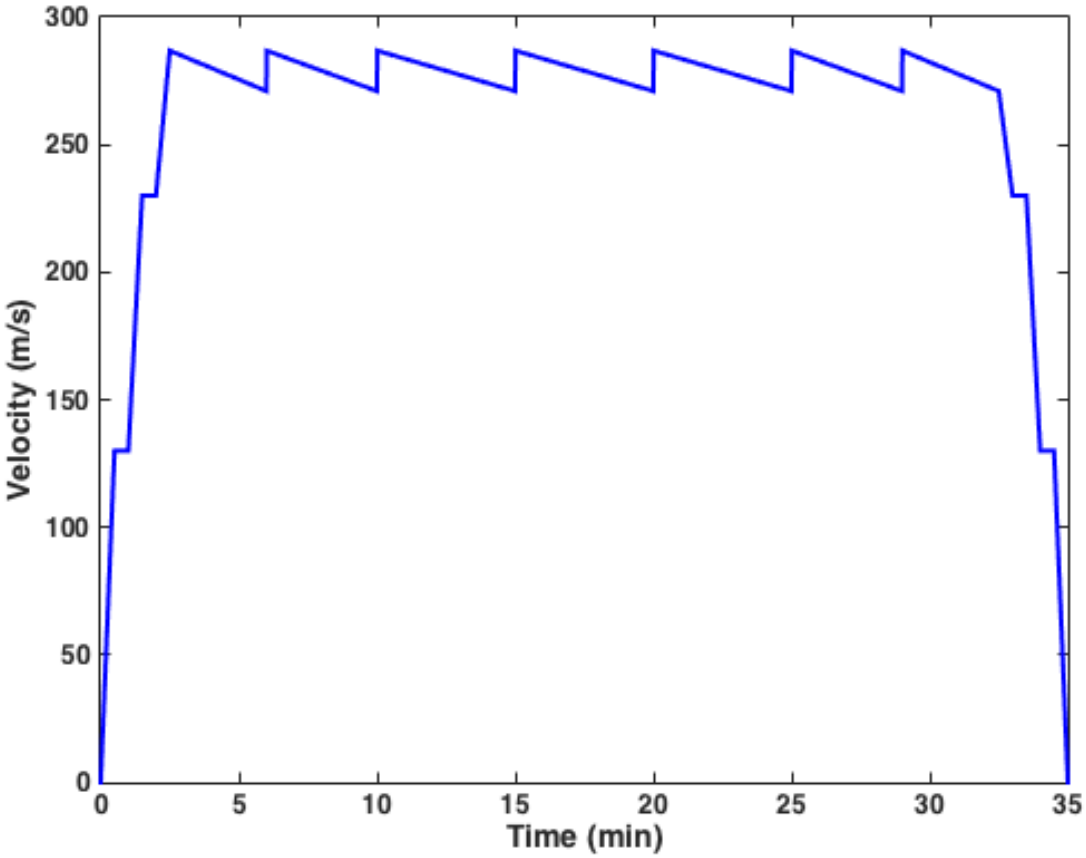

Figure 5: Notional Velocity Profile in Mission Analysis

where F_{thrust} is the net thrust generated by the flow through the pod nozzle, C_D [c4] is the pod drag coefficient, ρ is the free stream air density, S is the pod planform area, and D_{mag} is the drag produced by the magnetic levitation system. If the net thrust generated by the nozzle, then the acceleration equation is integrated to find the time and distance it takes for the pod to decelerate to the desired minimum speed using a predictor-corrector integration method [c5]

$$v_{i+1}^0 = v_i + f(v)\Delta t \tag{2}$$

$$v_{i+1} = v_i + \frac{f(v_{i+1}^0) + f(v_i)}{2}\Delta t \tag{3}$$

$$x_{i+1} = x_i + \frac{v_{i+1} + v_i}{2}\Delta t \tag{4}$$

The coast distance is used to determine the number of propulsive sections needed along the track to complete the mission. The energy is consumed in a single propulsive section is then multiplied by the number of flights determined from coasting distance to determine the electromagnetic propulsive energy consumed per flight during the coasting phase of the mission. The final phase of the mission is a constant linear deceleration of .5g from top speed to rest. Many systems driven by electromagnetic propulsion conserve energy through regenerative breaking.[2] For the sake of conservatism, it is assumed that there is no regenerative breaking in this process, although the model allows for regenerative breaking to be accounted for if the user desires. The energy consumed per flight is computed by adding the consumption of all three phases. The total yearly energy consumption is calculated based on the frequency of flights, which is determined by the user.

4. Cost

The cost module estimated the cost of energy, materials, pods, and construction capital. The cost of construction is highly subjective and is difficult to get an accurate estimation within less than an order of magnitude of uncertainty. However, the cost of materials and energy consumption can be estimate with significantly greater certainty. Thus, in this analysis, the cost estimations of materials and energy are of greater interest. According to the Electricity Information Administration, the average price of electricity is about .13 USD/kWh.[?] This is the electricity price that will be used for the model. Different electricity prices can be used for future analyses if necessary, but will not change the trends in the data this model produces. In addition to trade studies, a rough estimation of the ticket cost is included, which projects ticket cost based on the equation

$$Cost_{ticket} = \frac{(\frac{\partial Cost}{\partial L}L + \frac{\partial Cost}{\partial pod}n_{pods} + Cost_{capital}(1+ib) + \frac{\partial Cost}{\partial Energy}(Energy_{tube} + Energy_{pod}))}{n_{passengers} * \frac{pods}{s} * 3600\frac{s}{hr} * 24\frac{hrs}{day} * 365\frac{days}{year} * bm} \tag{5}$$

Where ib is the bond interest rate, bm is the number of years for bond maturity, and L is the total length of the track. Previous research indicated that construction costs are likely to be the largest cost factor in the system.[3] Due to the lack of a reliable method of estimating construction cost or ticket markup at this stage of the design process, the exact values of the ticket cost produced by this model will have a high level of uncertainty. However, the trade studies conducted in these analyses can provide useful information to inform the development of more accurate ticket cost models in the future.

B. Pod Level Component Descriptions

1. Drag

(Insert some description of CFD methods). CFD is performed on the pod to determine how the pod drag coefficient varies with Mach number [c1]. Figure 6 shows the CFD results for drag coefficient vs. Mach number. These results fit the trend expected for transonic flow given by the Prandtl-Glauert relationship. Drag Coefficient values will be interpolated from this data for each Mach number the system analyzes.

[c4] *Colin*: let's be sure to consistently use
[c5] *Colin*: do we need to include this equation at all?
[c1] *Colin*: this graph is missing

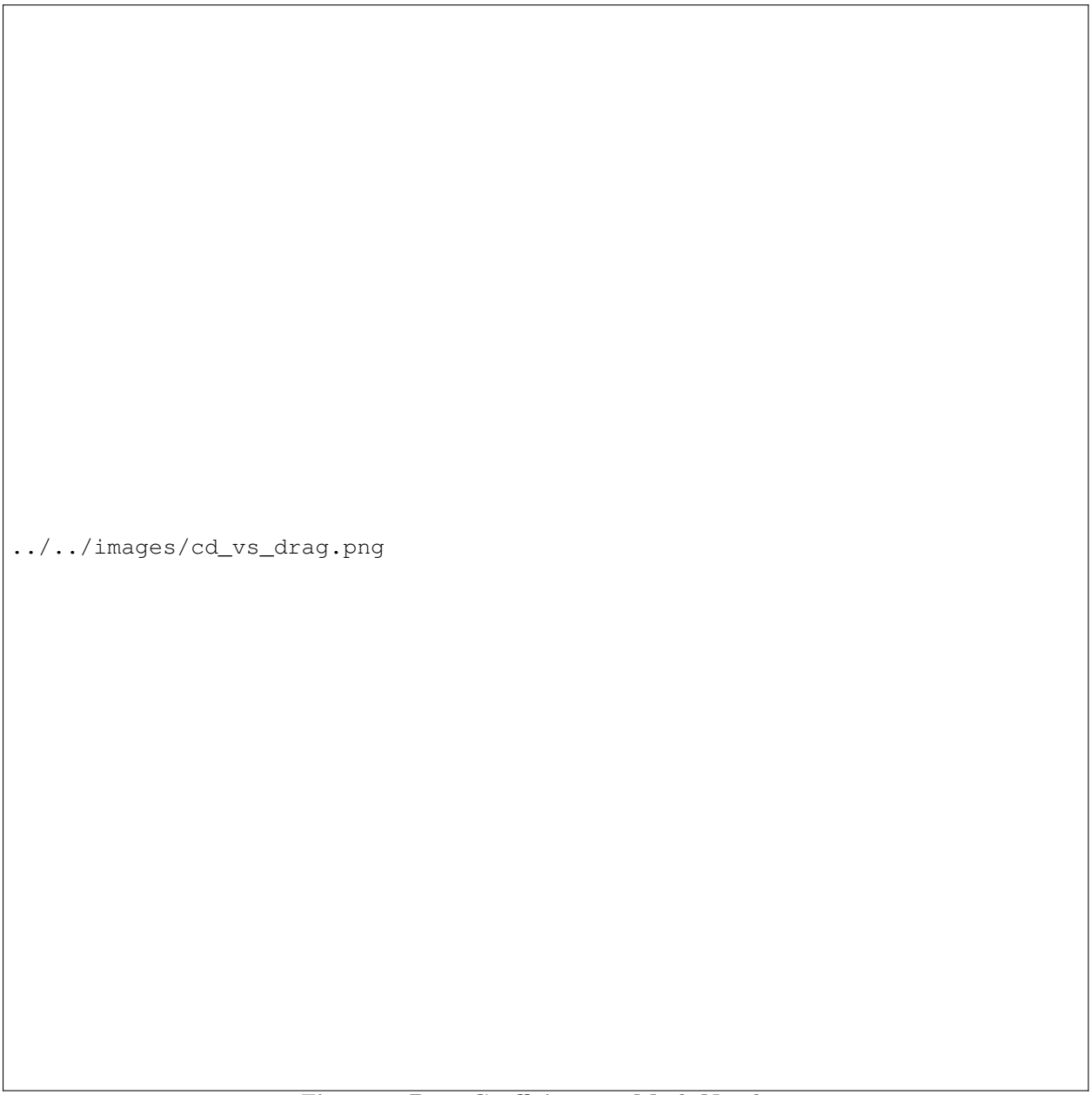

Figure 6: Drag Coefficient vs. Mach Number

2. *Cycle*

[c2]

3. *Drivetrain*

The Drivetrain module [c1] models an electric motor, inverter, and battery system. UBuilding off of previous work done at Georgia Tech and NASA, the module will compute the size and mass of both the motor and battery system neccesery to sustain the mission based on required torque and power demands over a mission profile.[4,5] We utilize a modified algorithm for sizing the battery from the algorithm developed at NASA by MK Bradley et. al. with the modification that the voltage of the battery as a function discharge is modeled using a polynomial fit to discharge curves provided by cell manufacturers.[5] We find this change provides results that are more flexible and specific to the leading commercial battery cells.

4. *Geometry and Mass*

The geometry and mass modules are simple in that they both primarily serve to add together mass and area values in previous modules. the geometry module adds the cross sectional area of the passenger section of the pod given by the user to the cross sectional area of the compressor exit duct, which is computed in the cycle analysis. The geometry module also estimates the thickness of the pod wall and the passenger compartment, then adds these areas together to compute the cross sectional area. The length of each component is also fed into the geometry model so it can compute the total pod length and planform area. The mass module takes the mass of each component and adds them with the total passenger mass in order to determine the mass of the pod without magnets for levitation. The Levitation component takes in this mass, computes the mass of the magnets, then outputs the total mass of the pods.

5. *Pod Mach*

[c2] The pod mach module uses the pod cross-sectional area, Mach number, and compressor inlet conditions to compute the tube area. As the pod travels, flow that is not entrained by the compressor must accelerate around the pod. Due to the pods transonic flight speed, it is possible that this bypass flow could accelerate to Mach 1 and cause the flow to choke, which would lead to an undesirable buildup of pressure in front of the pod and increased drag. To avoid this condition, this module sizes the tube area such that there is a large enough bypass area to prevent the bypass flow from accelerating to Mach 1. This is done using a simple quasi 1D area relationship for compressible flow given by the equation

$$\frac{A_1}{A_2} = \frac{M_2}{M_1}\left(\frac{1+\frac{\gamma-1}{2}M_1^2}{1+\frac{\gamma-1}{2}M_2^2}\right)^{\frac{(\gamma+1)}{2(\gamma-1)}} \tag{6}$$

For this analysis, M_1 is the free stream Mach number, M_2 is the desired bypass Mach number, A_1 is the initial area of the bypass flow (A_tube - A_tinlet), and A_2 is the bypass area (A_tube - A_pod). For these analyses, M_2 is set to .95 in order to provide a slight factor of safety to prevent the flow from reaching the choking condition [c3]. In order to make this model higher fidelity, it is possible to modify the areas in the relationship to account for boundary layer development over the pod outer surface. As the boundary develops, the effective bypass area is reduced which increases the risk of bypass flow reaching Mach 1. However, it is possible to modify this by increasing the effective pod radius by the displacement thickness of the boundary layer. The sensitivity of structural design to boundary layer growth is important and will be discussed at length later.

6. *Levitation*

The Hyperloop concept operates using a levitation system to significantly reduce friction during high velocity areas of travel. In this analysis, a passive magnetic levitation system is used to suspend the pod above the track as it travels. The passive system is advantageous because it requires zero power input for levitation to

[c2] *Colin*: does this section belong here?
[c1] *Colin*: are we going to call these by their OpenMDAO name i.e. 'Group' or something more generic like module?
[c2] *Colin*: need to consistently format table
[c3] *Colin*: We need to decide how to display symbols: nomenclature section at beginning or paper? Table at beginning of each section? Inline text descriptions following/preceding equation?

Table 1: Tube Power Variables

Symbol	Variable	Units
A	Area	m^2
A^*	Throat Area	m^2
none		
M	Mach number	none
γ	Ratio of specific heats	none
P_{crit}	Critical pressure at which bucking occurs	Pa
E	Elastic modulus	Pa
ν	Poisson Ratio	none
t	Thickness	m
r	Radius	m
δ^*	Displacement boundary layer thickness	m
x	Distance in x direction	m
Re_x	Length based Reynolds number	none
ε	expansion ratio	none
L	Track Length	m
ib	Bond interest rate	none
bm	Bond maturity	years
g	Gravitational acceleration	m/s^2
v	velocity	m/s F_x
Magnetic Drag	N	
m	Mass	kg
α	weighing factor	

occur, which is advantageous when traveling over long distances. The Inductrack passive levitation method developed at the Lawrence Livermore National Laboratory is chosen as the system for our Hyperloop model.[2] Some assumptions were taken to simplify the analysis adapted from this model. It is assumed that ferrite tiles were not used so that the added inductive loading is set to zero, leaving only the distributed inductance to computed in the model. Fringe fields from the magnetic array are also ignored in this analysis and the width of the magnetic array is set equal to the width of the track. These three simplifications and assumptions allow the overall scale factor for the total force, $levsf$ [c4], to set equal to unity.

The levitation group makes two critical calculations: the inductance of the track required for the pod to levitate at a desired speed and the mass of the permanent magnets onboard. The breakpoint levitation module uses a desired minimum levitation speed and uses it to calculate important track parameters, including the ratio of inductance to resistance of the track.

Using a desired levitation speed, the total mass of magnets required and drag force produced is is then calculated. The lift and drag produced produced by the magnets are given in the equations

$$F_y(\omega) = [\beta_0^2 w/(4\pi L dc\lambda)][(1 + R/\omega L)(1 + R/\omega L)^2)]Ae^{-4\pi h/\lambda} \tag{7}$$

$$D_{mag} = (m_{pod}g)R/\omega L \tag{8}$$

In these equations, the drag and the magnet mass are both functions of the magnet area and thickness. To minimize drag and mass, a Pareto optimization is performed prior to running the system model. The following cost function is developed by normalizing drag and mass, then multiplying by a weighing factor *alpha* and adding them together in the following equation[c1]

$$f(\alpha) = \alpha\bar{F_x} + (1 - \alpha)\bar{m_{mag}}v \tag{9}$$

[c4] *Colin*: levsf referenced but not defined?
[c1] *Colin*: is this the correcft equation?

Table 2: Symbols Used in Levitation Equations

Symbol	Use	Units
λ	Wavelength of Halbach Array	m
w	Width of the Magnetic Array	m
β_0	Halbach Peak Strength	Tesla
R	Resistance of the Track	Ω
L	Inductance of the Track	Henry
ω	Frequency of the Induced Current	Hz
h	Desired Levitation Height	m
g	Gravity	m/s^2
A	Area of Magnetic Array	m^2
v	Velocity of the Pod	m/s

Where the bar signifies the normalized value. The weighing factor *alpha* is chosen arbitrarily between zero and unity; high values of *alpha* emphasize minimizing drag while low values of *alpha* emphasize minimizing mass.

C. Tube Level Component Descriptions

Vacuum The vacuum subsystem is a group which evaluates two phases of the vacuum use: pump down and steady-state use. The pump down vacuum module evaluates the number of vacuum pumps and the energy required to pump the vacuum tube down from ambient pressure to the desired tube pressure in the amount of time determined by the user. This information is critical because the vacuum will need to be pumped down once tube is constructed and in the event of an emergency pressurization. The vacuum pump down model is given in the equation [c1]

$$InsertNatesVacuumEquation \tag{10}$$

[c2]add symbols and description of Vacuum equation The pump down energy and weight of pumps will be critical for cost and structural analyses. The Vacuum group also considers the vacuum energy consumed during the steady state run time of the system. In theory, if the tube is perfectly air tight, there would be no need for the vacuum to run at all once the tube is pumped down. However, some amount of leakage is inevitable, which will necessitate some amount of energy consumption by the vacuum pumps to maintain the desired tube pressure over time. The effect of leakage rate on energy consumption is critical and will be discussed in more depth later. For the purpose of this analysis, the vacuum is modeled as a compressor using the same pycycle2 component seen in the pod compression cycle analysis, with the same internal implicit solver.[?] The pressure ratio of the will be equal to the ratio of ambient pressure to desired tube pressure and the mass flow through the vacuum at steady state will be equal to the leakage rate.

Thermal Management [c3]section for thermal management/tube wall temp. Jeff needs to do this?[1]

Electromagnetic Propulsion A series of linear synchronous motors (LSMs) is proposed to accelerate the pod from rest to top speed and maintain top speed with periodic boosts. While the specifications of the LSM system design are beyond the scope of this analysis, the amount of energy and power required of an LSM can be determined using the simple mechanics relationship [c4]]

$$F_{net} = F_{LSM} + F_{thrust} - \frac{1}{2}C_D\rho V^2 S - D_{mag} \tag{11}$$

[c1] *Colin*: where is the vacuum equation?
[c2] *Colin*: *Text added.*
[c3] *Colin*: *Text added.*
[c4] *Colin*: sum of forces equation repeated when deriving acceleration of pod

In which F_LSM is the force required of the LSM system. This equation is integrated to determine the power and energy requirements for both startup and coasting booster sections. For the purpose of this analysis, the efficiency of the LSM is assumed to be .8.[?]

Structure The Structural analysis group determines the structural design of the tube for two phases of travel: travel over land and under water. When traveling overland, the tube is assumed to be supported by pylons above the terrain at a given height. For travel under water, the tube is assumed to be supported at a certain depth below sea level. The structural analysis in each phase is under constrained and allows for several free choices to be made by the user, which could have a significant impact on design configuration and material cost. To handle this challenge, the structural design of the tube at each phase will be optimized in order to determine the configuration that minimizes cost. The optimization methods will be discussed later in further detail.

D. Flow of Information

1. Top Level

At the top level, design parameters are passed from the user to the pod, tube, mission, and ticket cost subsystems which then all output variables to the user.

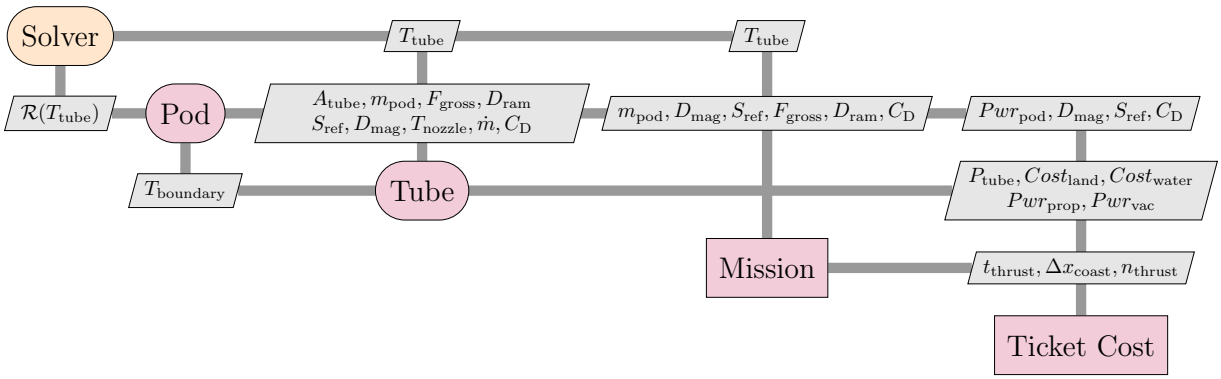

Figure 7: XDSM diagram for entire system model

2. Pod

3. Tube

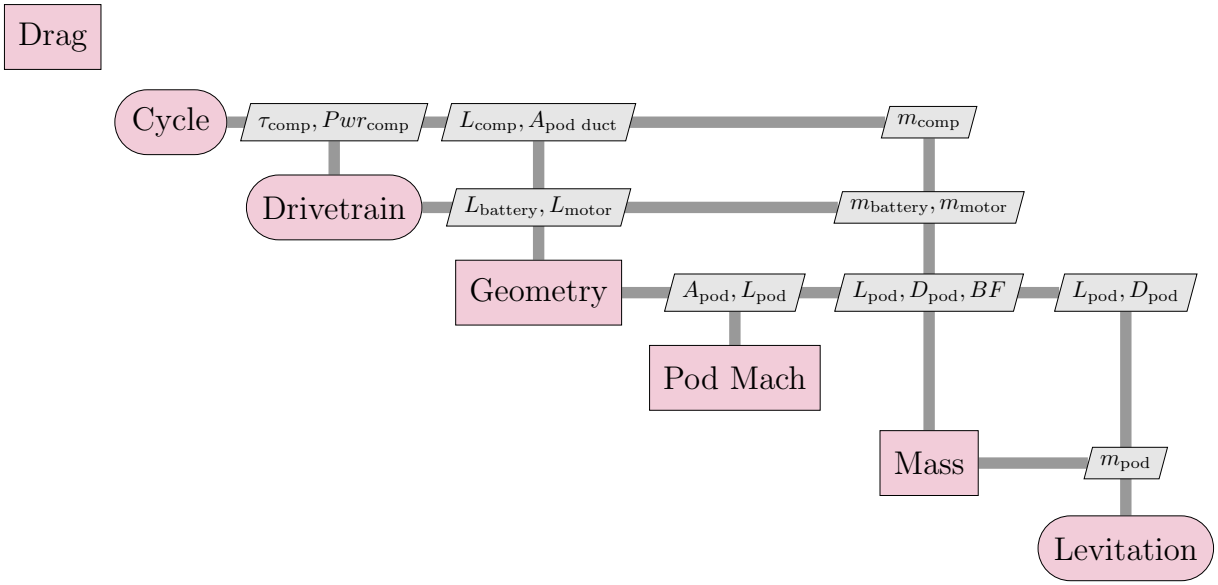

Figure 8: XDSM diagram for Pod group

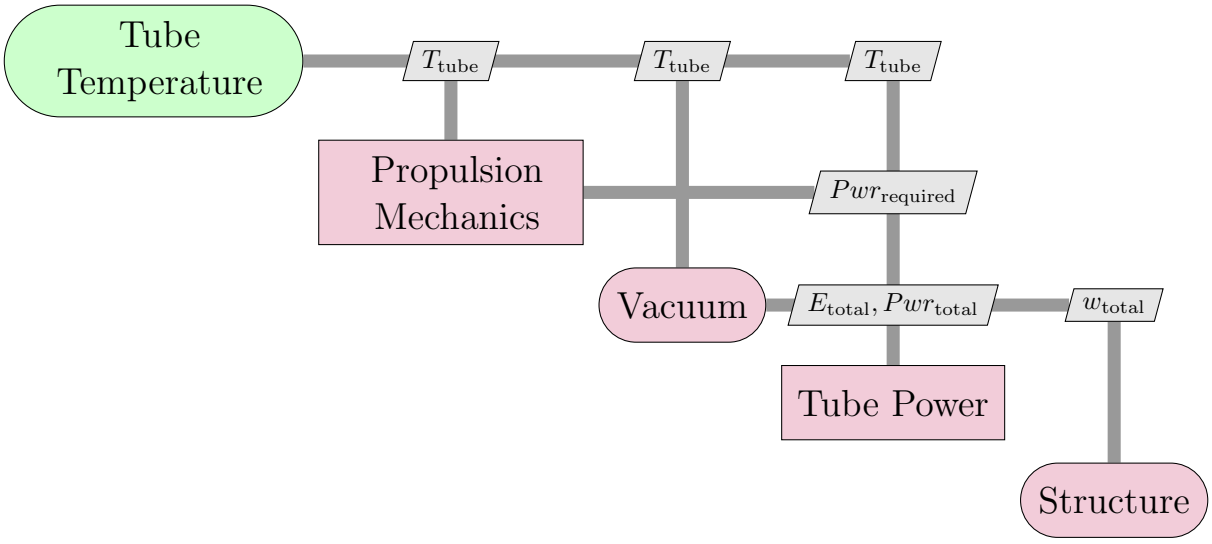

Figure 9: XDSM diagram for Tube group

IV. Subsystem Analyses and Optimizations

Subsystem Analyses and Optimizations

A. Structural Subsystem Optimization

Prior to analyzing the system as a whole, several analyses are performed on various subsystems in order to examine important design trades at the subsystem level and determine reasonable values for top-level design inputs. Structural analysis is performed on the tube as the pod travels both over land and under water. In these analysis, material properties of steel area used for the tube and material properties of concrete are used for the tube in order to illustrate trends. Both phases are analyzed prior to running the full system using values of design variables suggested from previous research with safety factors where appropriate.[1] Then, cost function optimizations are performed with appropriate design variables to determine which input values minimize material cost. These values will then be fed into the whole system model to perform trade studies on top-level design variables. It is understood that the values obtained by performing optimization on subsystems will likely not be optimal when the whole system is analyzed; however, these values are useful for illustrating physical trends and system trades. The ScipyOptimizer is used to minimize the scalar cost function using the Sequential Least Squares Programming (SLSQP) algorithm for gradient based optimization.[6,7] First, travel of the pod over land is analyzed. In this case, the pod travels within a tube that is suspended on pylons of a given height above the ground. To perform this analysis, multiple simplifying assumptions must be made. The tube is assumed to have thin walls relative to the tube radius and thus will be modeled as a thin-walled pressure vessel. The tube is assumed to be horizontal and the height of the pylons is assumed to be constant. This allows a section of the tube between two pylons to be modeled as a hollow cylindrical beam with simple supports at its ends. Each pylon is modeled as a beam fixed at the ground with axial and transverse loads applied to its end. The structure is designed according to beam bending equations with the sectional weight of the beam modeled as a distributed load and the mass of the pod as a point load at the beams center (the structure is analyzed with the pod at the center of the beam since this produces the highest bending stress in the tube). With these assumptions, two extreme structural configurations can be imagined: one in which the tube is thick but is supported by pylons that are spaced very far apart, and another in which the tube is thin but must be supported by many closely spaced pylons. A cost function is developed by adding the cost of the tube material and the cost of the supporting pylons per unit length, with the thickness of the tube and the distance between pylons as design variables as shown in the equation

$$Cost/Length = \frac{TubeCost}{kg} * m'_{pod} + \frac{PylonCost}{kg}\frac{m_{pylon}}{\Delta x_{pylon}} \tag{12}$$

Where m is the mass per unit length of the tube. This model, however, is incomplete because the pylons can be any arbitrary size. To fix this problem, the pylons are sized according to the buckling condition for a fixed column. Imposing the condition allows for the spacing of the pylons to be computed in terms of pylon radius and tube thickness using the equation

$$\Delta x_{pylons} = \frac{\frac{\pi^2 E r_p^4}{16h^2} - \frac{1}{2}m_{pod}g}{\frac{1}{2}m'g} \tag{13}$$

Using this relationship, the cost function is defined with the tube thickness and pylon radius as design variables. The final step is to appropriately constrain the optimization. The minimum radius of the pylon is computed based on the yield strength of the pylon material. Likewise, the minimum thickness of the tube is calculated using the buckling condition for vacuum cylinders given by the equation?

$$P_{crit} = \frac{\gamma E}{4(1-\nu^2)}(\frac{t}{r})^3 \tag{14}$$

For this analysis, the area of the tube is varied and the pylon spacing will is recorded for different of pod masses. Figure 10 shows that pylon spacing decreases significantly as tube area increases. This is reasonable because, as tube area increases and becomes heavier, larger pylons are needed to support the heavier load and a thicker tube is needed to handle higher bending stress, both of which increase cost. This optimization shows that moving the pylons closer together mitigates this cost penalty. When performing analysis at

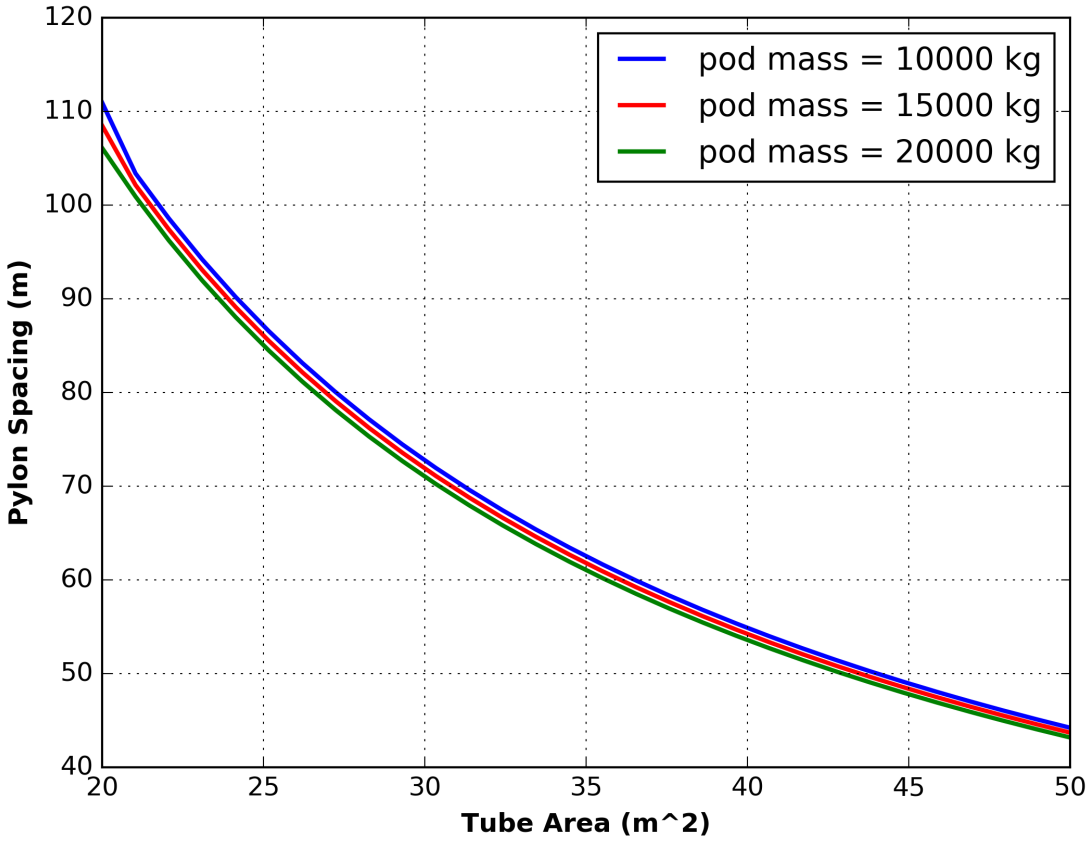

Figure 10: Optimal Pylon Spacing vs. Tube Area

the top level of the system, this plot along, with the pylon buckling constraint, will be used to determine reasonable inputs for tube thickness and pylon spacing for any given tube area or pod mass in order to reflect optimal structural design conditions as closely as possible. These results also give us preliminary insight into how favorably the Hyperloop structure scales with pod capacity. For any given tube area I this regime, increasing the pod mass from 10,000 kg to 20,000 kg results in a change in pylon spacing of less than 2%, with the sensitivity of pylon spacing to pod mass decreasing for higher tube areas. This suggests that the mass of the tube is dominant when sizing the structure of the system and that the pod mass is negligible in this regime. This means that the capacity of each pod can be increased with negligible ramifications on structural design. Pod capacity trades will be discussed in greater detail in the following sections. However, this analysis shows that pod capacity can be greatly scaled up with minimal impact on structural design or the cost of materials and construction. Structural analysis is also performed for underwater travel. The model will have to be altered slightly from the model of the pod over land in order to account for buoyancy. In this case, a section of the tube is modeled as a hollow cylindrical beam subjected to a distributed load equal to the difference between the sectional buoyancy and the sectional weight. Travel underwater could have an interesting effect on structural design because it is possible for the tube to be sized such that the entire weight of the structure is suspended by its own buoyancy. In this case, support structure would only be necessary to stabilize the structure against changing tides, currents, and seismic activity rather than support the structural load [c1].

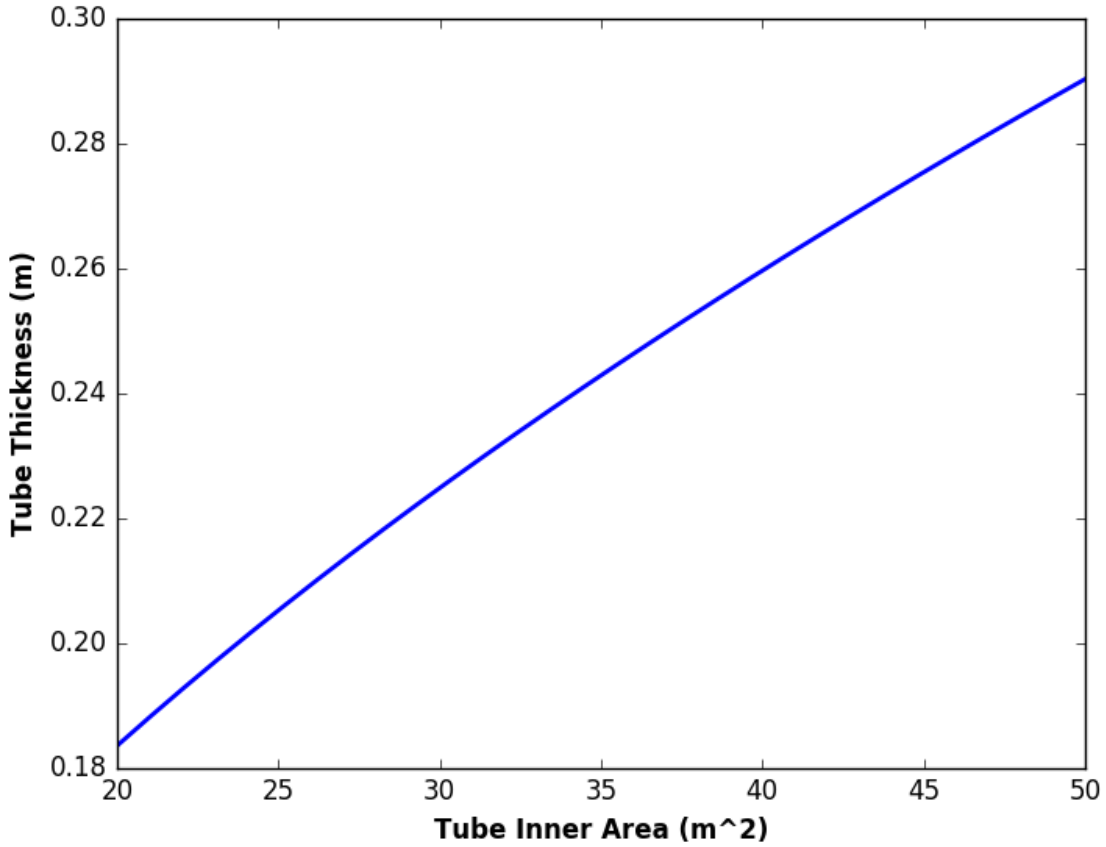

Figure 11: Thickness for Self-Suspension vs. Inner Area

Figure 11 shows the tube thickness at which the buoyant force is equal to the weight of the tube allowing the tube structure to support itself. Points above this curve will have weight greater than buoyancy and thus will require pylons to support the weight. Likewise, points below this curve will result in a buoyant force that is greater than the weight of the tube and would require structures to anchor the tube at a certain

[c1] *Colin*: need the thickness vs self-suspension graph

depth.

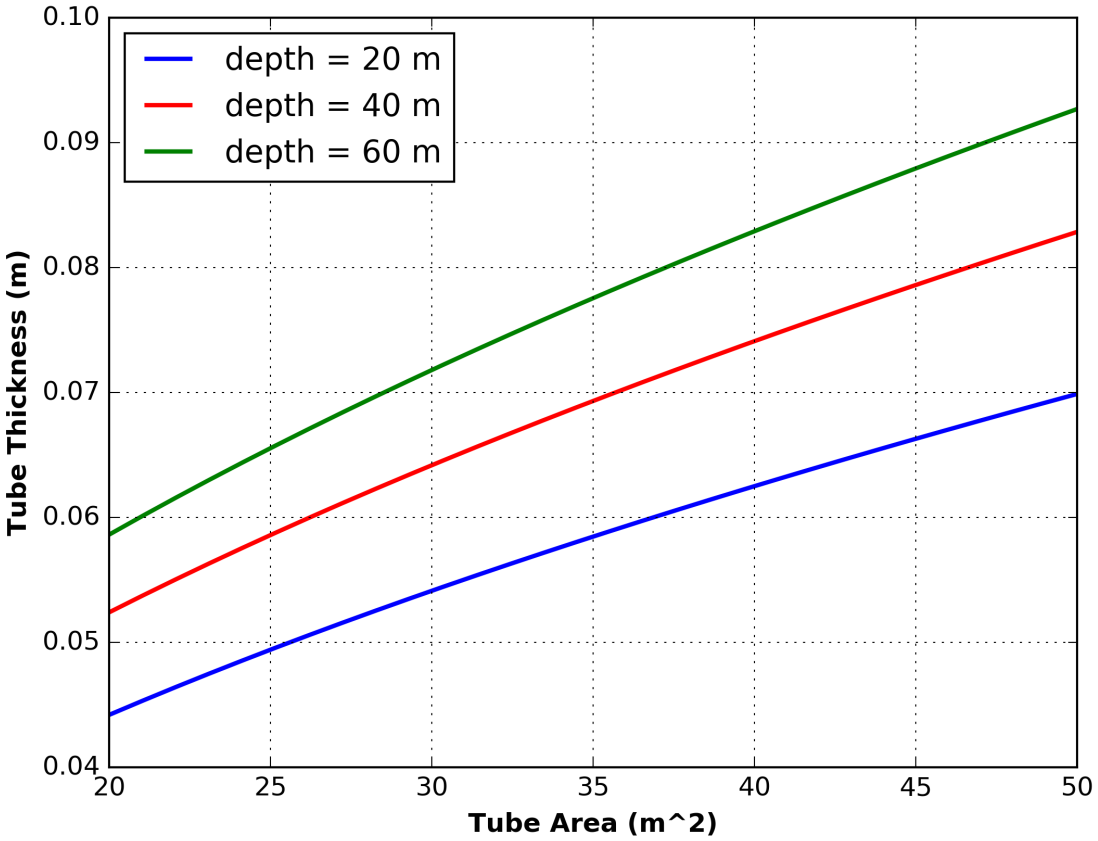

Figure 12: Tube Thickness vs. Tube Area of Travel Under Water

Traveling under water, unlike over land, allows the ambient pressure to change significantly with the depth. Figure 12 shows the sensitivity tube thickness to tube area for multiple different values of depth. For large depths, thickness increases with tube area at a faster rate, which results in increased material cost. It is important to note that the thickness values calculated in this analysis are significantly below the values necessary for self-suspension given in fig. 11. Thus, for underwater phases, it can be concluded that the Hyperloop structure would likely be subjected to a buoyant force greater than the weight of the system and would need to be designed in such a way that the pod is anchored to the sea floor and stabilized in the event of disturbances. The structural trade studies shown here suggest that there could be significant benefits to traveling underwater as opposed to over land. The depth could be chosen such that the tube could be thinner. Furthermore, it will likely be easier to make the a straighter path traveling underwater because there will be less buildings and features to contend with. Since the tube needs to be air-tight regardless of whether travel is underwater or overland, either phase will likely require the same level of manufacturing cost. While evaluating the exact cost differential is beyond the scope of this paper due to the subjective and volatile nature of capital cost evaluation, this system model suggests that there could be real benefits from traveling underwater and should be the subject of further research.

B. Pod Frequency

The traffic between the notional end points and the market demand for tickets at a given cost will determine the amount of passengers the Hyperloop must be able to accommodate in a given period of time. The number of passengers per unit of time that the Hyperloop can transport is equal to the number of passengers per pod times the frequency at which pods depart. If a constant pod capacity is assumed, then the only way to accommodate for periods of high demand is to increase the frequency at which pods depart. It is

important to understand the limitations of pod frequency in order to obtain a reasonable sense of maximum passenger throughput. There are three factors that must be considered when evaluating limitations on pod frequency: safety, the amount of time it takes to board, and the number of pods available. Pods must be spaced out such that each pod can slow down and stop before hitting the pod in front of it in the event of an emergency stop. Simple linear acceleration equations can be used to determine the minimum distance separating to allow for deceleration and are shown below [c1]

$$InsertLinearAccelerationEquations \tag{15}$$

Assuming a braking deceleration of 1g, a Mach number of .8, and a tunnel temperature of 320 K,[1] the minimum distance between pods is calculated to be 4.2 km with no safety margin. At top speed, the deceleration time is calculated to be 29.2 s. This means that, with no safety margin, the maximum pod frequency is about 2 pods per minute. This frequency should easily be satisfied, even with a safety margin, due to the time that must be allowed for passengers to board. It is likely that passengers will need considerably more than 30 seconds to board, meaning that safety is not likely to be the the factor limiting maximum pod frequency. Finally, in this analysis, it is assumed that the operator must have enough pods to fill the entire tube when launching flights at a given frequency. Consequently, having less time in between pods reduces the distance in between pods, which increases the number of pods required to fill the tube and sustain the desired pod frequency. Due to these three limiting factors, lower pod frequencies are desirable because they increase the safety margin in the event of emergency braking, increase the time passengers have to board, and reduce the number of pods that the operator must have in order to sustain a given pod frequency. The effects that changes in pod capacity will have on system design and performance will be discussed in further detail later in this study.

C. Boundary Layer Sensitivity

In this system model, the tube cross section is sized such that the flow in the pod does not choke. Previous models attempted to impose this condition by assuming that the area of the bypass flow is equal to the tube cross sectional area minus the pod cross sectional area (cite NASA paper). This model attempts to build upon previous models by also accounting for the development of a boundary layer over the pod surface. The boundary layer formation further reduces the bypass area and increases the chance of choking in the flow. Thus, a larger tube will be necessary to prevent choking when boundary layer effects are accounted for, which will increase the costs of both raw materials and construction. This model will first analyze the sensitivity of the tube cross sectional area to the boundary layer growth along the pod surface. Then, estimations of boundary layer thickness as a function of length-based Re will be made in order to analyze the sensitivity of tube cross sectional area to changes in pod length. For each analysis, the tube is sized using the previously discussed inviscid, quasi-1D area relationships for compressible flow. To account for the boundary layer using this method, the boundary layer is modeled as a cylindrical ring with a thickness equal to the maximum thickness of the displacement boundary layer, δ^*, over the outside of the pod, effectively reducing the area of the bypass flow. Using this model, the contraction of the bypass flow is given by the equation

$$\varepsilon = \frac{A_{bypasseff}}{A_{bypass}} = \frac{A_{tube} - A_{pod} - \pi((r+\delta^*)^2 - r^2)}{A_{tube} - A_{inlet}} \tag{16}$$

This relationship accounts for the reduction in bypass area due to a boundary layer of arbitrary displacement thickness. First, the sensitivity of tube area to displacement boundary layer thickness is studied over a range of boundary layer thicknesses for various pod cross sections. Next, the model uses a flat plate approximation to obtain a relationship between boundary layer and length. Since $Re > 500,000$, the boundary layer is assumed turbulent with a velocity profile[?] [c1] [c2]

$$NEEDVELOCITYPROFILEEQ \tag{17}$$

[c1] *Colin*: Ken needs to add these equations, couldn't find them
[c1] *Colin*: need citation for Fox and McDonald
[c2] *Colin*: need velocity profile equations from Ken

Using this boundary layer velocity profile, the thickness of the displacement boundary layer is derived using a similarity solution to produce the equation[?]

$$\frac{\delta^*}{x} \approx \frac{.04775}{Re_x^{1/5}} \tag{18}$$

The system model uses there to relate displacement boundary layer thickness, and therefore tube area, with pod length. It is understood that these equations do not accurately represent the physical relationships in our model because they are derived in the textbook by Fox and McDonald assuming 1D flow over a flat plate with zero pressure gradient. Characterizing the displacement thickness of the boundary layer in 3D conical flow is beyond the scope of this analysis. However, the approximation made in this analysis is useful for studying how tube area and material costs may change with increasing pod length within an order of magnitude of accuracy. The pod configurations tested in each analysis is given in [c1]need to add pod config table. Figure 13 indicated the effects that displacement boundary layer has on the cross sectional

Table 3: Configurations in boundary layer sensitivity study

Figure 13: Tube Cross Sectional Area vs. Displacement Boundary Layer Thickness and Pod Cross Sectional Area

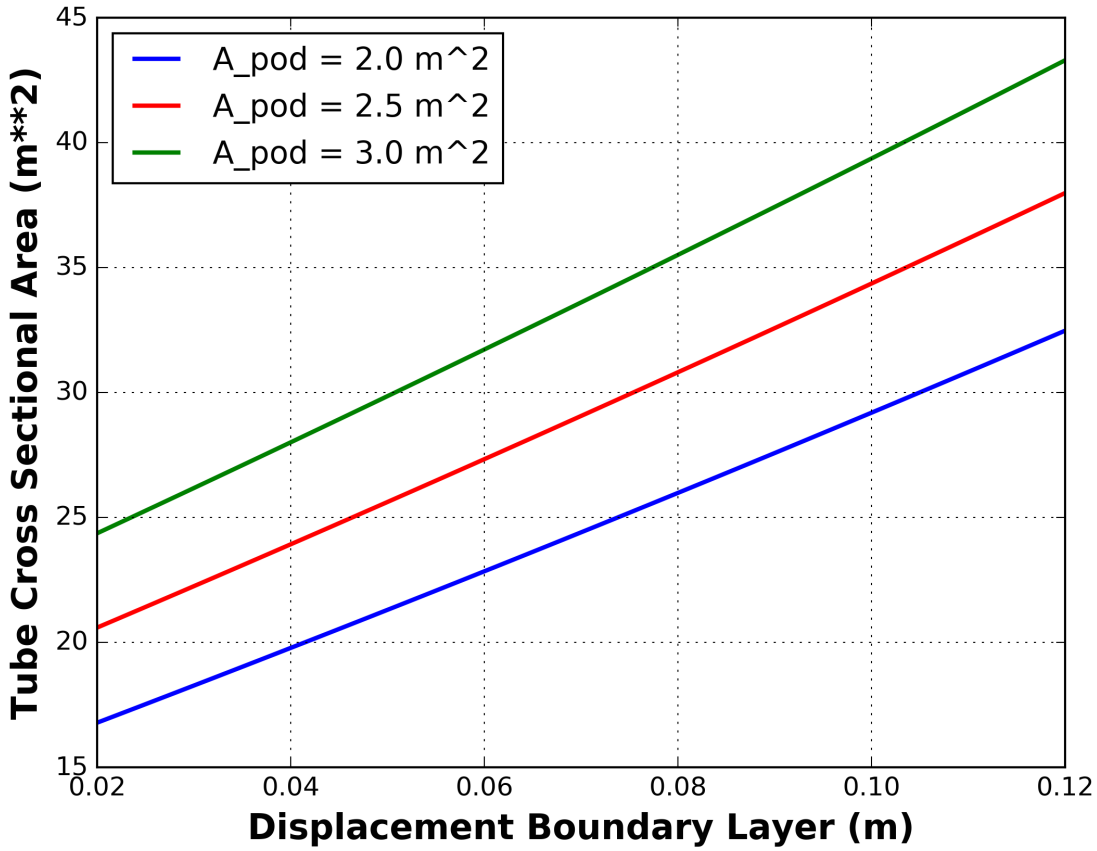

area of the tube. It is shown that the cross sectional area of the tube increases rapidly as the thickness of the displacement boundary layer increases. For $A_{pod} = 2 \times 10^2\,\mathrm{m}^2$, a 1 cm increase in δ^* results in an increase of approximately $1.57\,\mathrm{m}^2$ in A_{tube}. Thus, it can be inferred that the tube area, and therefore the tube material cost, are extremely sensitive to boundary layer thickness. Furthermore, the rate of increase of the tube cross sectional area also increases with pod cross sectional area. This relationship exists because more bypass is area is lost as pod radius increases for a given displacement boundary layer thickness. This

[c1] *Colin: Text added.*

means that the coupling between tube and pod cross sectional areas is even stronger than was indicated in previous research. Figure 14 shows the necessary cross sectional area of the tube as a function of pod

Figure 14: Tube Cross Sectional Area vs. Pod Length

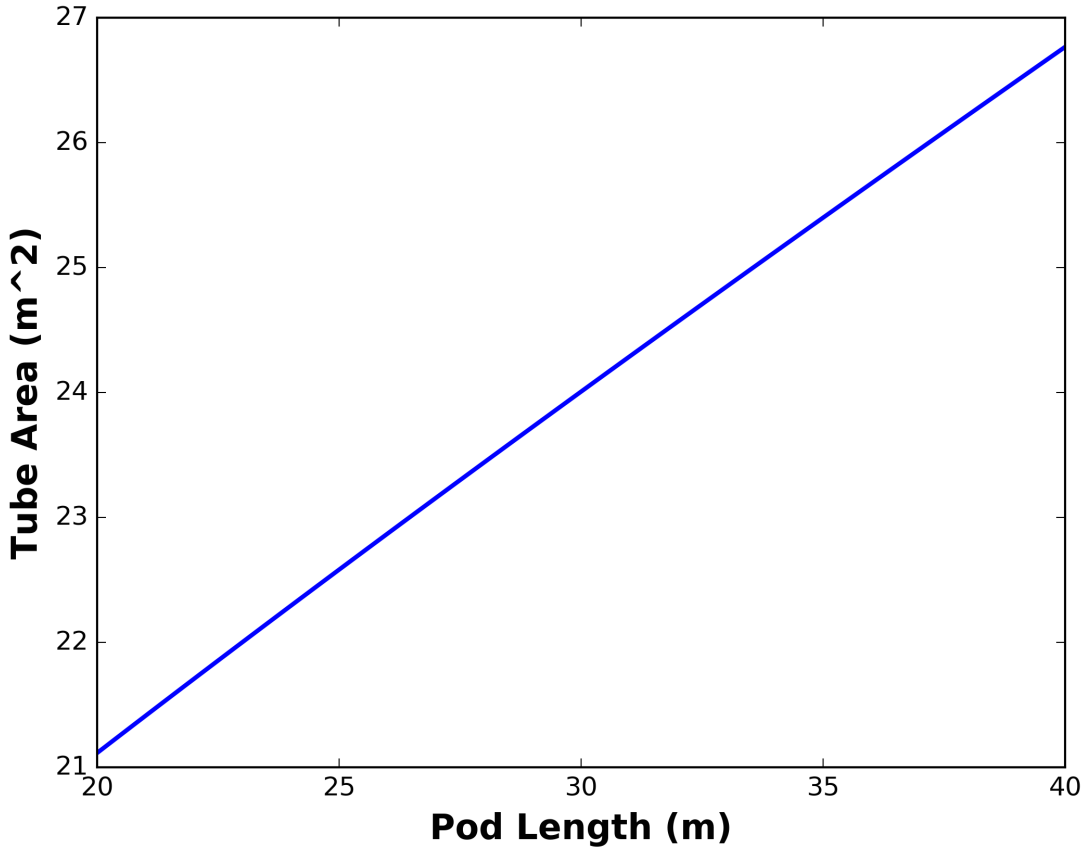

length using the previously described relationship approximation. It is shown that increases in pod length due to higher passenger capacity, increased battery length, more compressor stages, etc. require the tube cross sectional area to increase in order to accommodate for larger boundary layer growth. This relationship reveals a coupling between tube cross sectional area and pod length that has not been accounted for in previous system models. The tube area is highly coupled with boundary layer thickness due to its effect on effective bypass area. Due to the sensitivity of tube area with respect to boundary layer thickness, it is important to develop a model that can accurately determine the displacement boundary layer thickness over the pod surface in order to avoid undesired choking or development of shock waves in the tube. Moreover, this analysis suggests that active flow techniques, such as boundary layer suction, which reduce boundary layer thickness could be very beneficial. Since the lowest tube cross sectional area is desired for a given pod configuration, boundary layer suction could reduce the size of the tube necessary to prevent choking which will reduce the total material and construction costs of the system.

V. Results

A. Mach Number Trades

It is known that the cost of the pod infrastructure is highly coupled with the Mach number at which the vehicle travels. In order to obey the choking constraint, higher Mach numbers will necessitate a larger tube to prevent the flow around the pod from accelerating to the speed of sound. This increases the material cost of the tube and the energy required to pump down the tube. In this analysis, the full system model will be run for a range of Mach numbers. For each Mach number, the area of the tube is recorded along

with total energy cost. In this analysis, the leakage rate is assumed to be a constant mass flow on the order 1 kg/s. This value should be sufficient for illustrating the trend of energy consumption as a function of Mach number. Different values of leakage rate will not significantly alter the trend, but will instead directly scale the amount of energy used by the vacuum system in a steady state condition. Figure 15 Indicates the

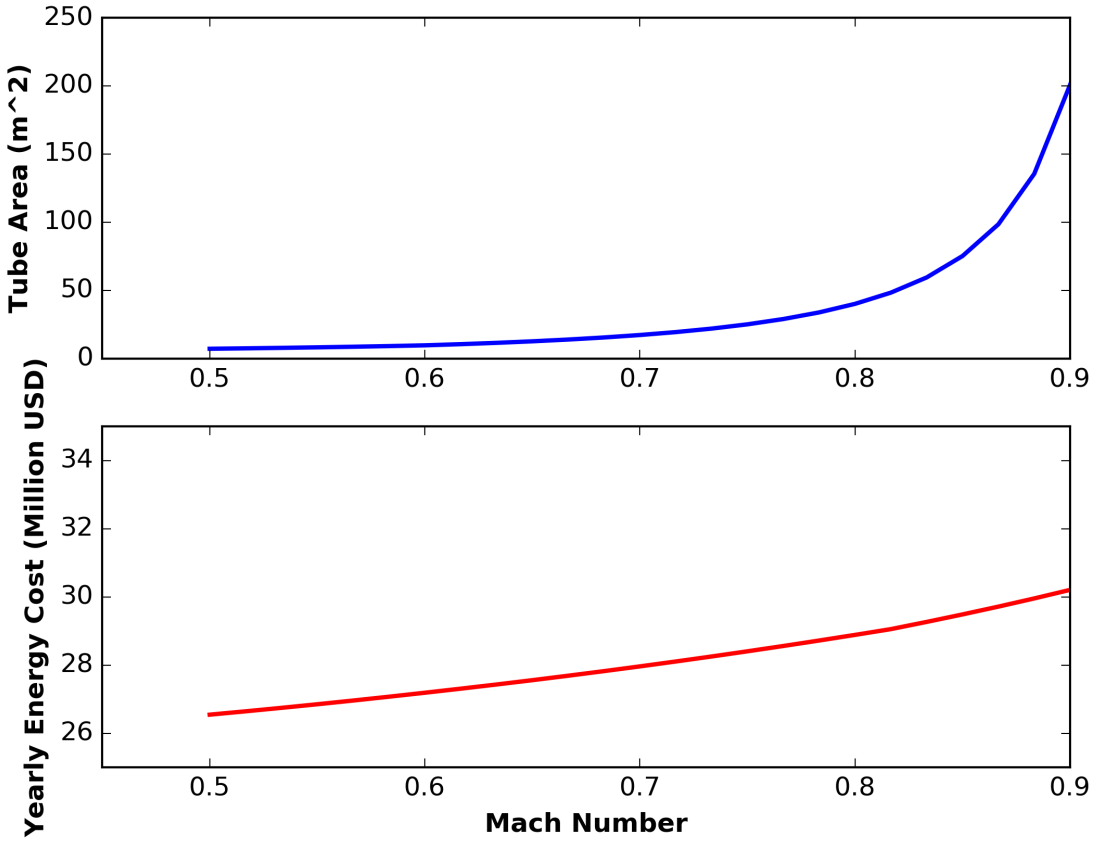

Figure 15: Tube Area and Yearly Energy Cost vs. Mach Number

how tube area and energy consumption change over a range of Mach numbers. As is indicated in previous research, tube area begins to increase rapidly around Mach .8.[1] Beyond this Mach number, small increases in Mach number result in a large increase in tube area, which will have a large impact on capital cost and pump down energy of the system. Conversely, fig. 15 indicates that there is very little marginal material cost required to increase Mach number. The increase in energy consumption is much more modest; however, the mild increase in energy cost is dominated by the increase in material cost for higher Mach numbers. Based on these results, it is estimated that any system level optimization of cost with respect to Mach number will result in a Mach number near .8. For this reason, a Mach number of .8 will be used in subsequent analyses to obtain reasonable evaluations of design trades and system behavior.

B. Pressure Trades

One of the most critical design variables of the Hyperloop is the tube pressure at which it operates. A lower pressure increases the power required of the vacuum system in order to pump the tube down and maintain tube pressure for a given leakage rate. However, it is known that the pressure at which the tube operates will increase the density of the air and thus increase the power requirements of both the electromagnetic propulsion system and the onboard compressor. As compressor power demands change, the length and mass of the motor and battery will change the pod geometry. Tube area is coupled with pod length, as was shown in the boundary layer analysis, while the power required of the electromagnetic propulsion system is coupled with pod mass. The boundary layer that was described previously is used for this analysis. Tube pressure is

perhaps the single most important design variable to understand because it is coupled with so many different aspects of system construction and performance. Trade studies using this fully comprehensive system model can provide valuable insight into the effects that variations in pressure have in every aspect of design and performance at the system level. Previous research has suggested that the ideal operating pressure should be on the order of 100 Pa.[1,3] However, such a low pressure could be costly and difficult to implement across such a larger stretch of tube, especially if there is significant leakage. It is likely that slight increases in tube pressure could result in significant decreases in energy consumption that could make up for increased drag penalty. To evaluate this, the full system model will be run for a range of pressures. Tube area, compressor power, steady state vacuum power, and total yearly energy consumption are recorded at each pressure. Other relevant design variables in this analysis are listed in the Table 4 [c1]table detailing design vars. Figure 16 shows tube area as a function of tube pressure. As pressure increases, tube area decreases

Table 4: FIX THIS

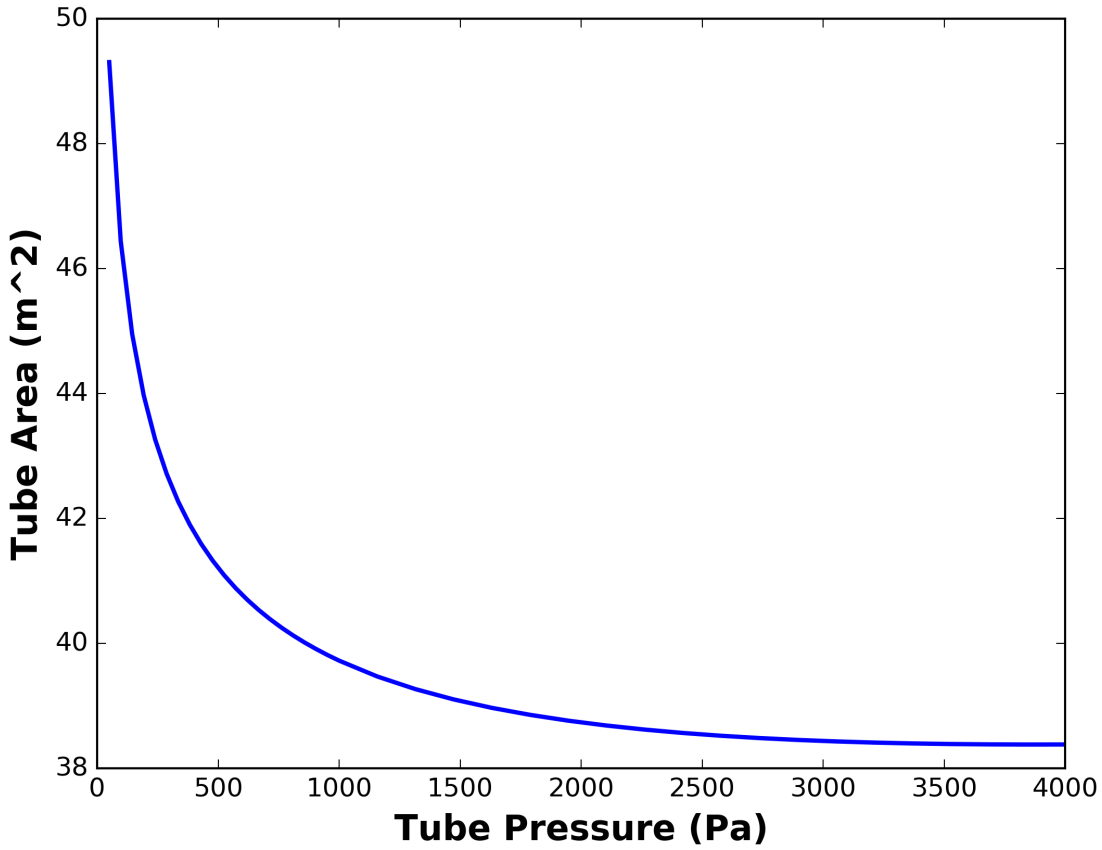

Figure 16: Tube Area vs. Tube Pressure

until leveling off around 3500 Pa. This relationship is due to the effect that pressure has on boundary layer thickness. Increasing the pressure increases the Reynolds number per unit length, which decreases boundary layer thickness. As boundary layer thickness is reduced the effective bypass area is increased which allows the tube area to be reduced for the same Mach number. However, compressor power increases linearly with pressure, which results in an increase pod length to hold a larger motor and battery. As was shown previously, increasing length results in increased boundary layer growth and causes tube size to grow. This trade results in two pressure regime, which are illustrated in fig. 16. At lower pressures, marginal increases in pressure result in decreases in tube area because the increase in Reynolds number per unit length dominates the length increases necessitated by higher compressor power demands. Meanwhile, at higher pressures,

[c1] *Colin: Text added.*

increases in pod length begin to dominate boundary layer sizing and the marginal effect on tube area is tempered. Figure 17 shows how the power and energy consumption change with tube pressure. As expected,

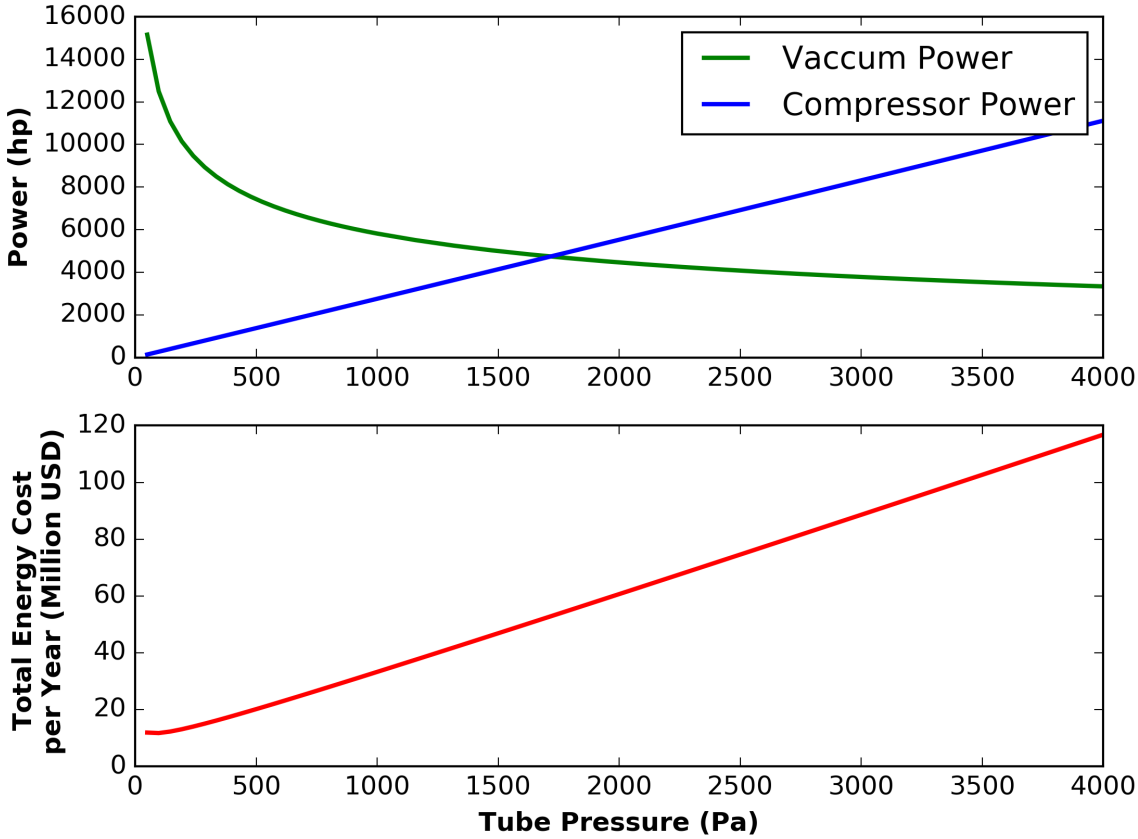

Figure 17: Power Demands and Energy Consumption vs. Tube Pressure

high tube pressures require lower power for a given leakage rate while requiring a higher power output from the onboard compressor for a given compressor ratio. Thus, energy cost increases for very low pressures due to the vacuum system and increases for very high pressures due to increased power demand from the compressor. The second plot in fig. 17 shows that this relationship produces a pressure at which energy cost is minimal. In this case, the energy consumption is minimal at about 100 Pa. Energy consumption increases fairly rapidly as pressure is increased beyond this minimum value. It is important to note that this exact value is dependent on the leakage rate, compressor pressure ratio, and whether or not regenerative breaking is used to recover battery energy (no regenerative breaking is assumed in this analysis). However, this relationship is crucial because it means that there does exist a pressure that optimizes energy cost and that energy cost can increase rapidly if deviations from this optimum point exist. A higher fidelity model can be used to determine exactly what value of pressure optimizes energy consumption for a given configuration. A more detailed examination of the effects that leakage has on optimum pressure will be conducted next.

C. Leakage Rate

A major goal of this model is to study the effect that leakage has on optimal tunnel configuration. The Hyperloop infrastructure will be designed and manufactured with the goal of making the tube air tight; however, a perfectly air tight tube is likely not possible. Slight leakage flow rates are to be expected due to diffusion, desorption, permeation, leaks through micro cracks, and leaks in mechanical mechanisms. Furthermore, air will likely need to be introduced to the system to allow passengers to board. The leakage rate due to diffusion and permeation is proportional to the tube surface area while the air introduced into the system during passenger boarding is proportional to the size of the boarding area and the frequency at

which pods are boarded by passengers. Thus, it is reasonable to assume that leakage rate is proportional to pod size and the frequency at which pods leave the station. While the exact leakage rate into the system is difficult to quantify, accounting for leakage provides valuable insight to performance of the system as a whole. The previous trade study showed that, for a given leakage rate, an operating pressure exists at which steady state energy consumption is minimal. This is because an increase in pressure decreases the energy required by the vacuum pumps to maintain tube pressure while increasing the energy required by the compressor system onboard the pod to compress higher mass flows. The pressure at which this minimum occurs is a function of leakage rate. To evaluate the sensitivity of optimum pressure to leakage rate, the previous study will be repeated for a range of leakage rates. In each study, the pressure at which minimum energy consumption occurs will be determined using the ScipyOptimizer. The minimum value of total energy cost and the corresponding tube pressure will be recorded and plotted to evaluate the effects that leakage rate has on the system design variables. For this analysis, the values of other relevant design parameters are listed in [c1] table for other design parameters?. Figure 18 shows the pressure at minimum energy consumption vs. the

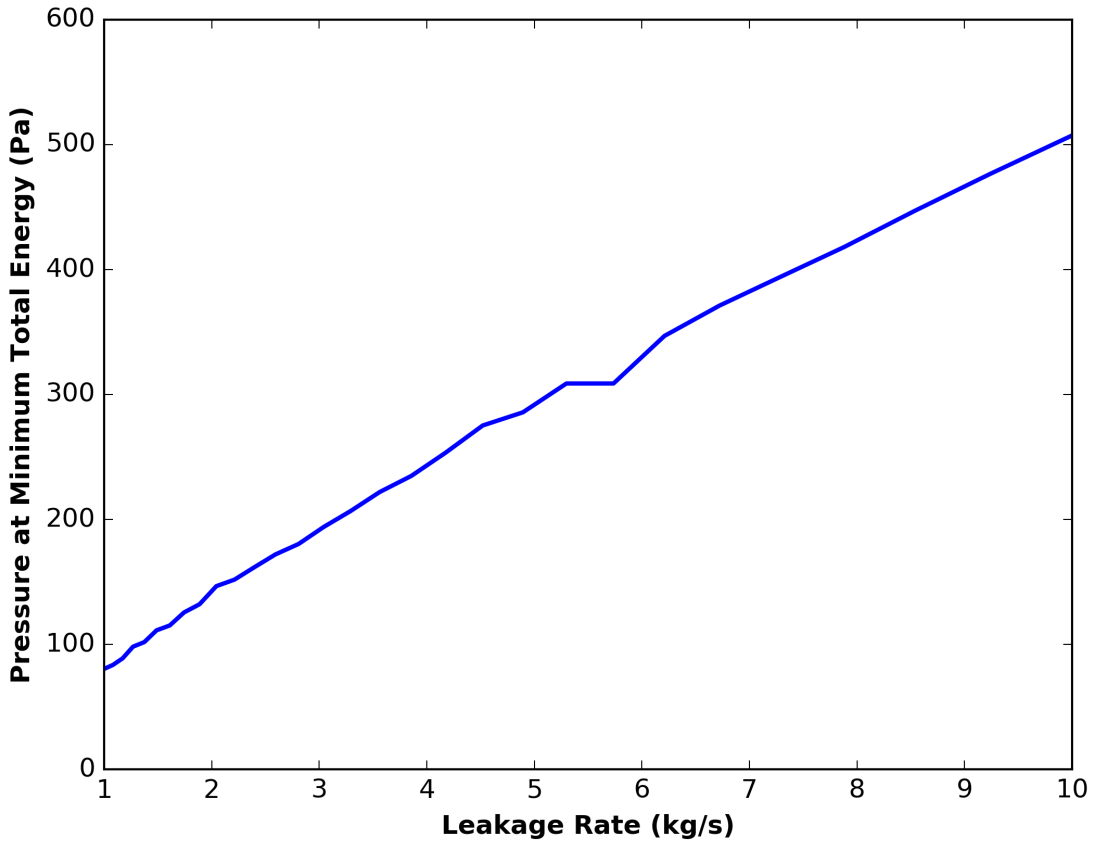

Figure 18: Pressure at Minimum Energy Consumption vs. Leakage Rate

leakage rate of the tube. The tube pressure that optimizes cost increases as leakage rate increase. This trend is reasonable because increasing leakage rate increases the power required for the vacuum pumps to maintain the tube pressure, which is offset by increasing the pressure that the vacuum is required to maintain. This relationship is critical because it reveals a coupling between tunnel leakage and energy consumption that system designers must consider. As fig. 18 reveals, changes in leakage rate can have a significant effect on energy consumption and energy cost. Increasing leakage rate causes minimum energy consumption to increase significantly, with the cost increase being even more substantial when operating at a suboptimal pressure. If the designer wants to optimize the system by minimizing the energy consumption, then more accurate modeling or empirical studies will be necessary to determine operating pressure. Furthermore, the

[c1] *Colin: Text added.*

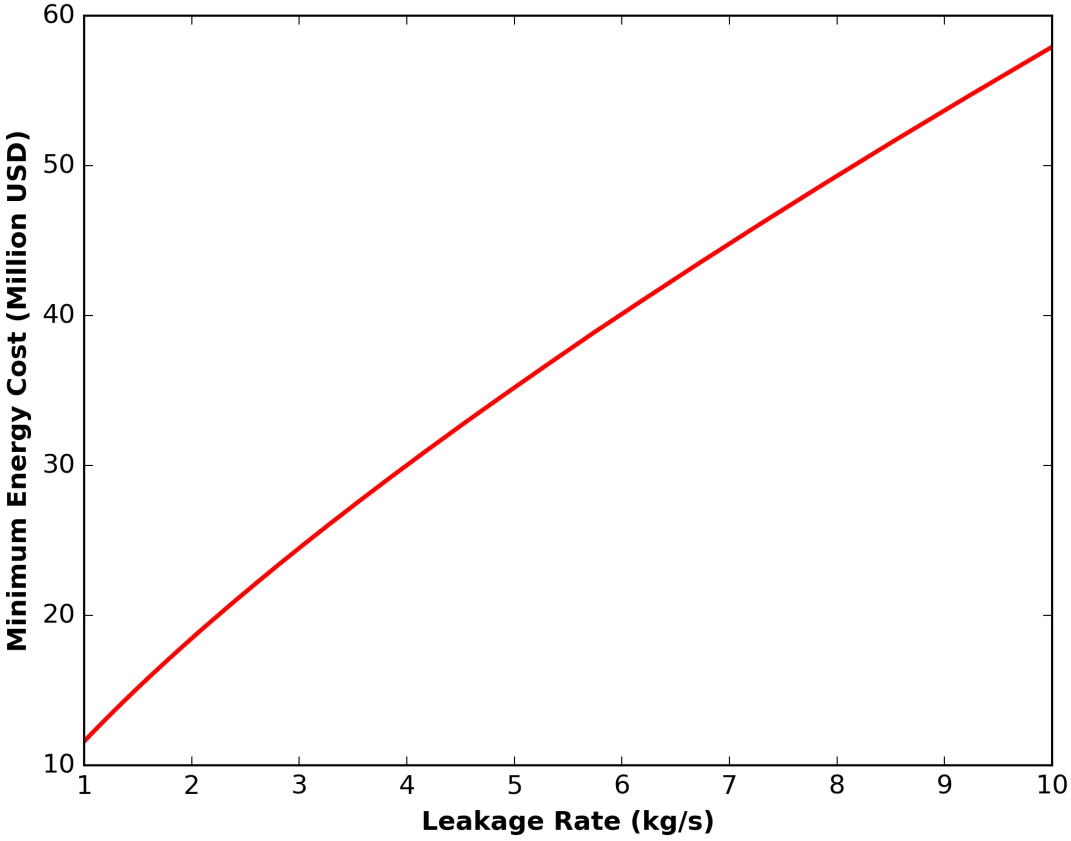

Figure 19: Minimum Energy Cost vs. Leakage Rate

assumption made in this study that leakage rate is constant is likely not indicative of a real system. As pod frequency changes, the leakage rate, and therefore the optimal pressure of the tunnel, is also likely to change. It may be possible for system designers to account for variable tube pressure when sizing the battery, compressor motor, and tube diameter in order to give the operator flexibility to change the tube pressure with pod frequency. This would allow the Hyperloop system to adapt to changing operating conditions to more closely track optimal design configurations in real time. Further research with higher fidelity modeling is necessary to further characterize the benefits of variable tunnel pressure as it relates to pod frequency and leakage.

D. Capacity Trades

Previous research analyzing the performance of the Hyperloop system suggested that the pod would likely be able to carry about 28 passengers.[3] To meet the market demand, the frequency at which pods departed could be increased or decreased as necessary. Increasing pod frequency too high could be problematic as this could require a large number of pods to be maintained at the end points and may not provide enough time for passengers to board comfortably. Thus, it is of particular interest to examine how the performance of the system is affected over a range of pod capacities. Increasing the capacity would allow the user to have fewer pods taking off at a lower frequency in order to carry the market demanded number of passengers per year. The overall benefits of changes in pod capacity can be more accurately determined by analyzing the sensitivity of energy consumption and operating cost to pod capacity. In this analysis, the number of passengers is varied over an order of magnitude. At each quantity, the energy cost and estimated ticket cost are recorded. Other relevant design variables are given in [c1]need to add the table giving design variables. Figure 20 shows

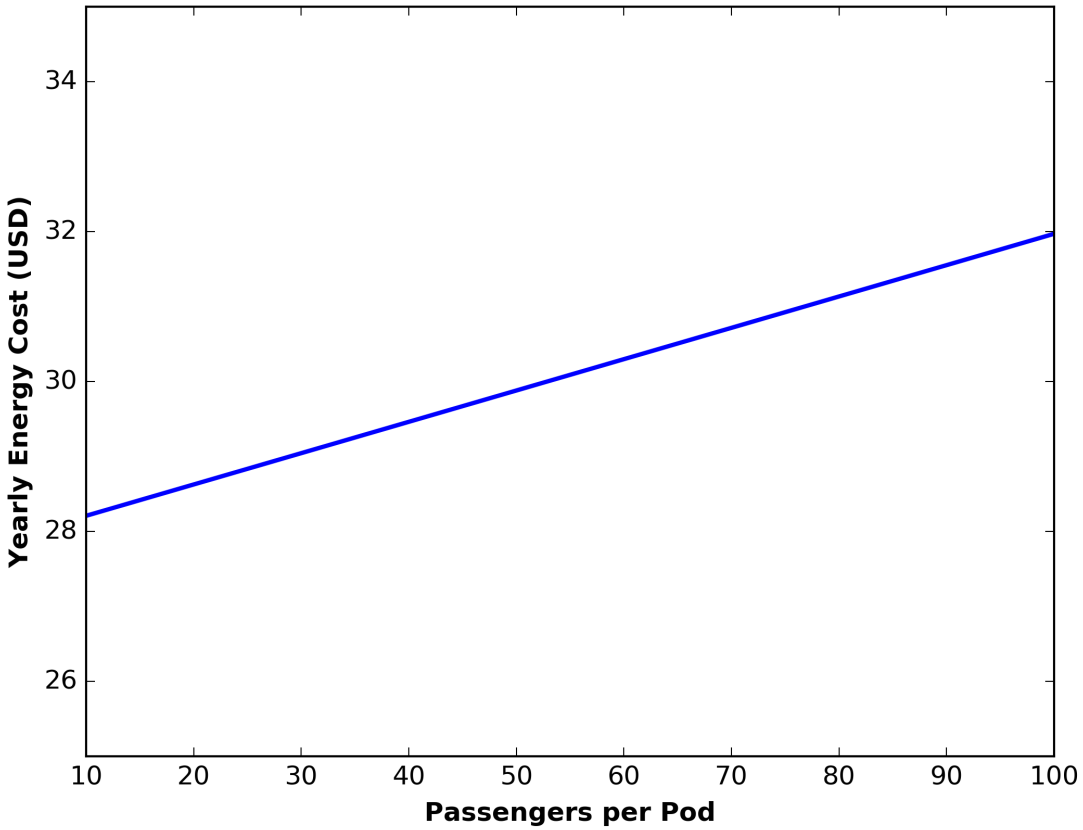

Figure 20: Yearly Energy Cost vs. Passengers per Pod

the relationship between yearly energy consumption and the number of passengers per pod produced by

[c1] *Colin: Text added.*

the system model. It is shown that, for the given operating condition, an order of magnitude increase in pod capacity only results in a 15% increase in yearly energy consumption. This, in conjunction with the previously discussed structural analysis, indicates that the cost associated with changing pod capacity is small. This relationship is significant because it means that the Hyperloop operator can specifically set the pod capacity to whatever value is necessary to meet a particular market demand without costly changes in performance or design. Furthermore, this makes it possible for future researchers to consider making Hyperloop pods modular. It is possible that, instead of having one large pod carrying a fixed number of passengers, the operator could have multiple pods that carry a small number of passengers each link together until the capacity of each individual flight reaches the value required by the market. This would allow the Hyperloop to handle high densities of passengers during peak travel times without having to increase pod frequency to prohibitive levels. Then, during lighter travel times, the operator could link fewer pods together to reduce the gross weight of each flight in order to reduce unnecessary energy consumption. The performance of the Hyperloop system scales favorably with pod capacity, which could potentially allow the system to be optimized to meet the demands of the market with little cost to operator.

VI. Conclusion

Using openMDAO and pyCycle2, a fully open source model of the Hyperloop concept was created to evaluate engineering trade studies at the top level of the system. The analyses presented illustrate the sensitivity of the overall system design and performance to several key design variables. First, it is shown that the coupling between tube pressure and the energy consumption of different system components result in the existence of an optimal tube pressure at which total energy consumption is minimal. This optimal pressure and minimum energy consumption are shown to be coupled to the tunnel leakage rate. Second, this paper supports previous research that traveling above Mach .8 is likely not practical because it requires a large tube size. The coupling between tube size and boundary layer growth is analyzed to show that the required size of the tube is very sensitive to boundary layer growth. As a result, further research on the modeling and implementation active flow control is recommended due to its potential to significantly reduce required tube size. Finally, the system is shown to scale favorably with pod capacity. This allows each pod to carry more passengers than was previously proposed, meaning the pod capacity can be optimized to meet market demand without prohibitive costs to the operator. Although this work is not high fidelity, the trends and trade studies identified provide valuable insight into the physics behind the Hyperloop concept and how these physical relationships can inform future design efforts. The open source, modular nature of this system model will allow future researchers to modify, adapt, and improve the model to include more specific subsystems and higher fidelity modeling as needed. The modeling platform is intended to serve as a publicly accessible baseline that is easy to expand and delve deeper into this unique multidisciplinary system.

VII. Appendix

A. Model Overview (Continued)

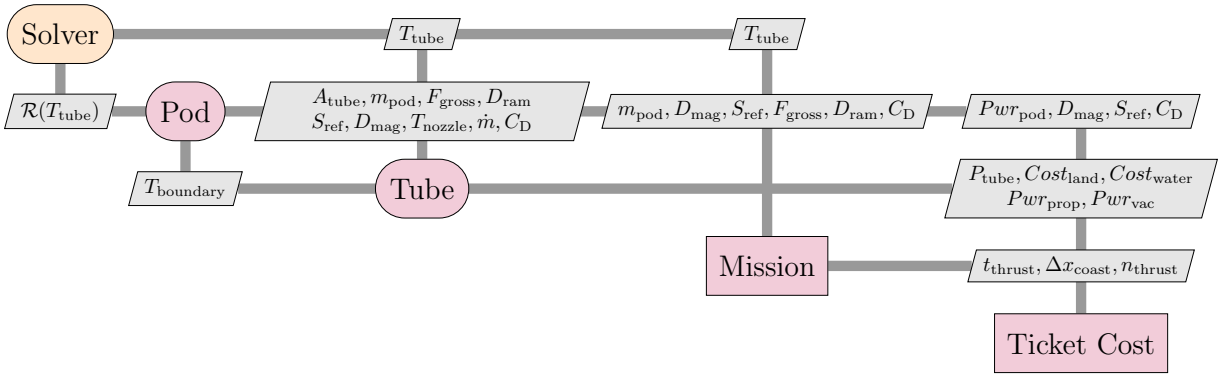

Figure 21: XDSM diagram for entire system model

A. TubeGroup

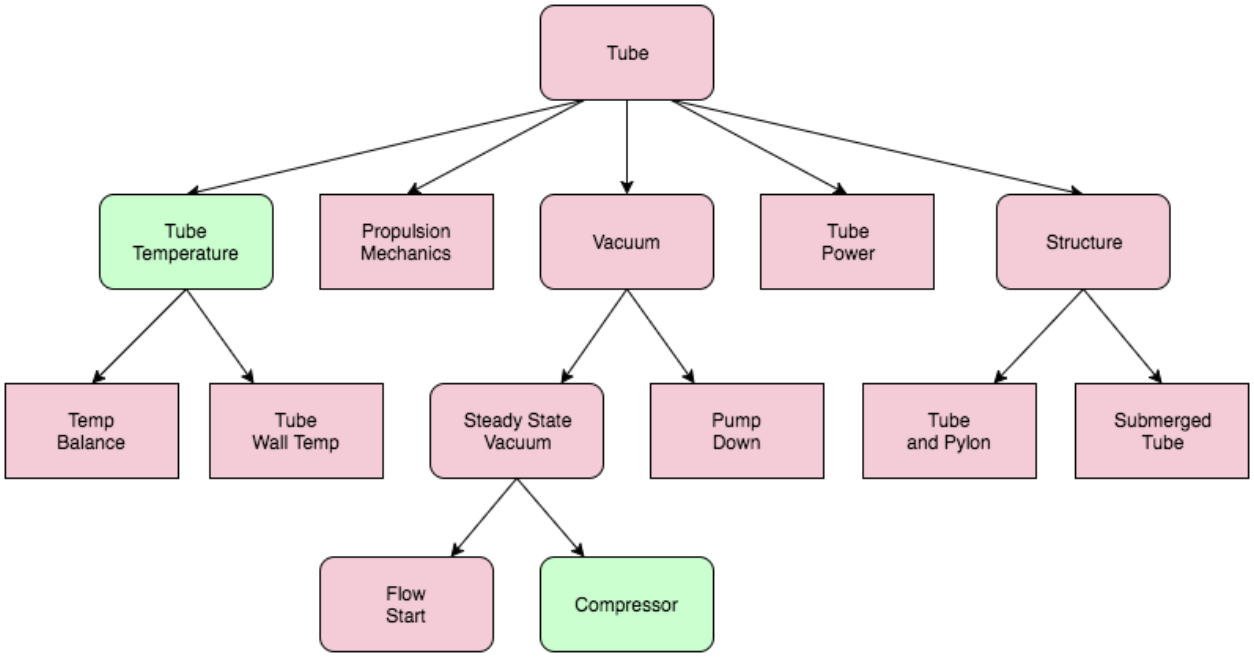

Figure 22: Hierarchial tree digram showing structure of TubeGroup

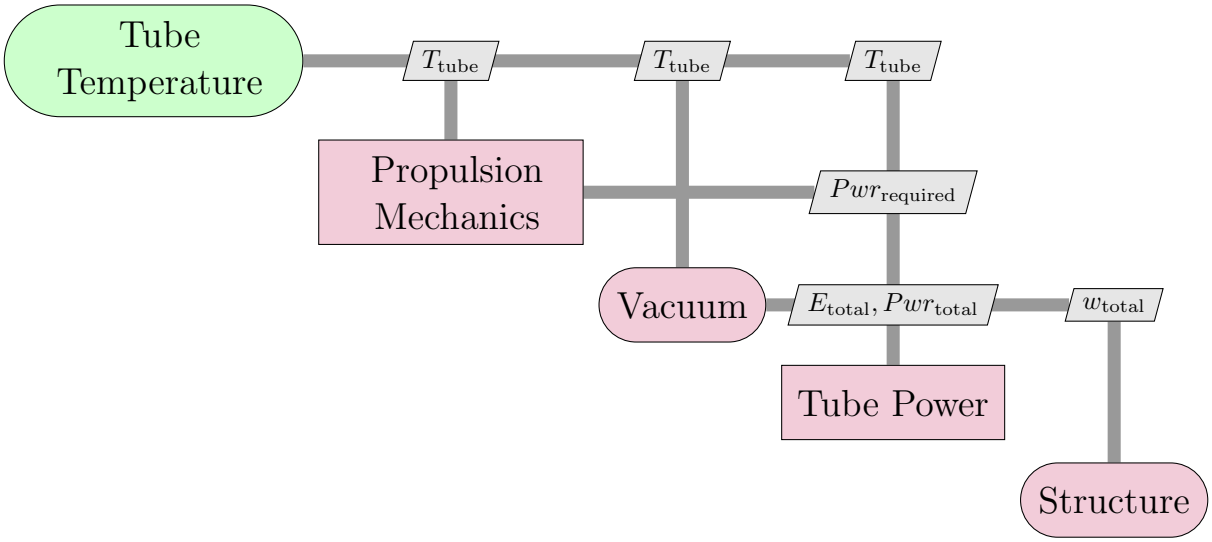

Figure 23: XDSM diagram for Tube group

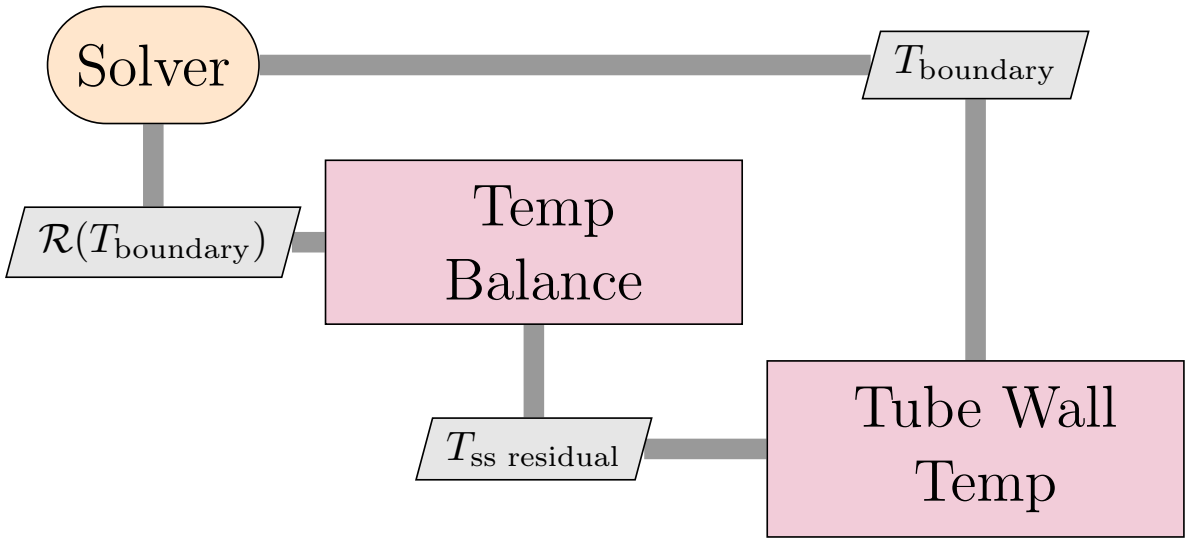

Figure 24: XDSM diagram for TubeTemp group

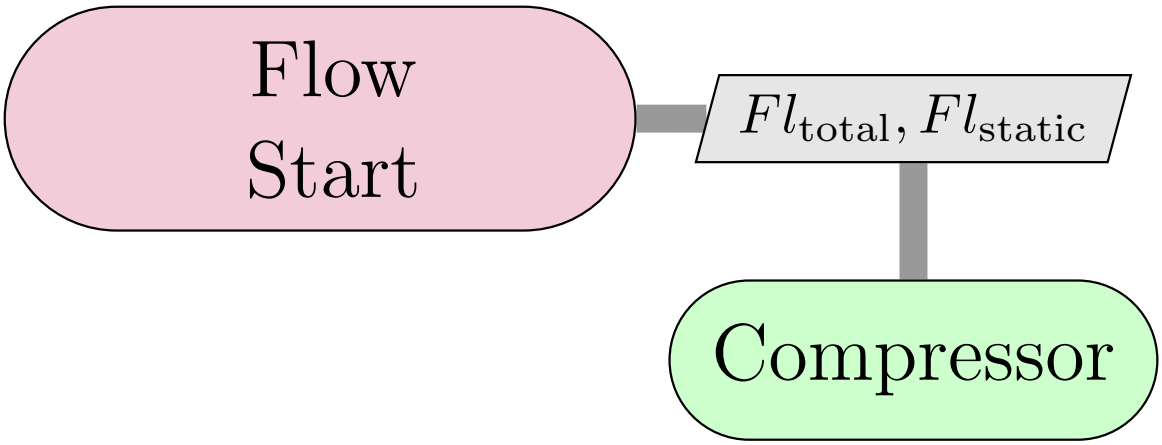

Figure 25: XDSM diagram for SteadyStateVacuum group

A. PropulsionMechanics

B. TubeTemp

1. TubeWallTemp

2. TempBalance

C. Vacuum

1. SteadyStateVacuum

1.1 FlowStart

1.2 Compressor

2. PumpDown

D. TubePower

$$Pwr_{prop} = Pwr_{prop,once} * n_{thrust} \tag{19}$$

$$E_{prop} = Pwr_{prop} * t_{thrust} \tag{20}$$

$$Pwr_{tot} = Pwr_{vac} + Pwr_{prop} \tag{21}$$

$$E_{tot} = E_{vac} + E_{prop} \tag{22}$$

$$Cost_E = Pwr_{tot} * Price_{elec} \tag{23}$$

E. Structure

1. SubmergedTube

2. TubeAndPylon

Table 5: Tube Power Variables

Symbol	Variable	Units
$Cost_E$	Energy cost	USD/h
E_{prop}	Energy required for pod propulsion for trip	kWh
E_{tot}	Total energy required from tube/grid	kWh
E_{vac}	Energy required for vacuum system	kWh
n_{thrust}	Number of boosts required for trip	none
$Price_{elec}$	US average for electricity price (2015)	USD/kWh
Pwr_{prop}	Power required for propulsion system for trip	kW
$Pwr_{prop,once}$	Power required to accelerate pod once	kW
Pwr_{tot}	Total power required from tube/grid	kW
Pwr_{vac}	Power required for vacuum system	kW
t_{thrust}	Thrust time	s

B. PodGroup

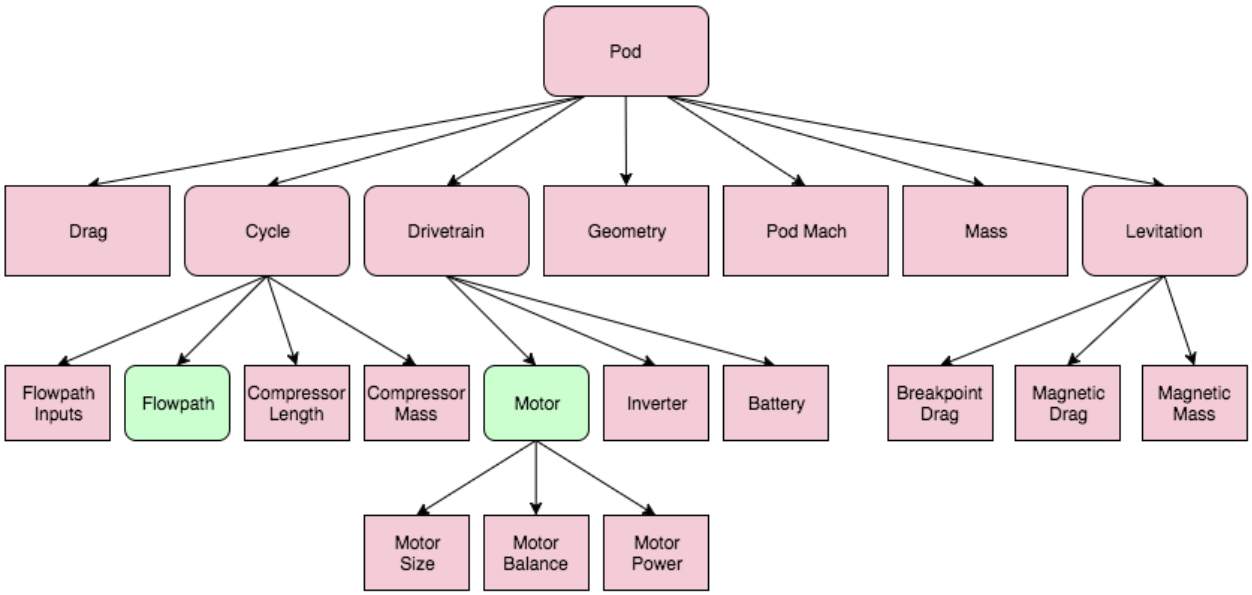

Figure 26: Hierarchial tree digram showing structure of PodGroup

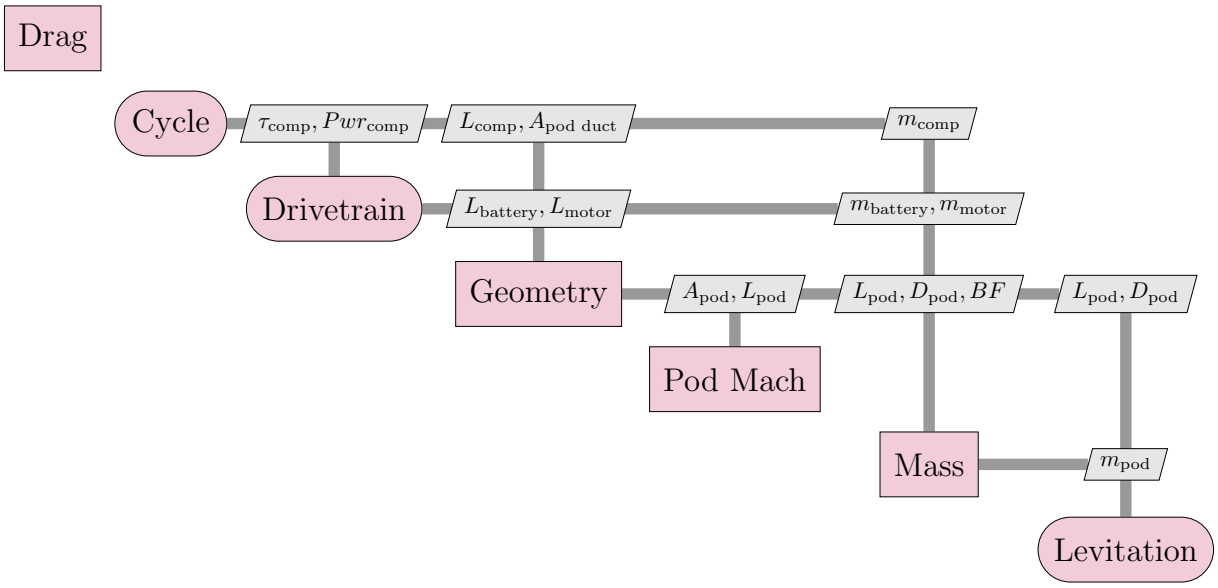

Figure 27: XDSM diagram for Pod group

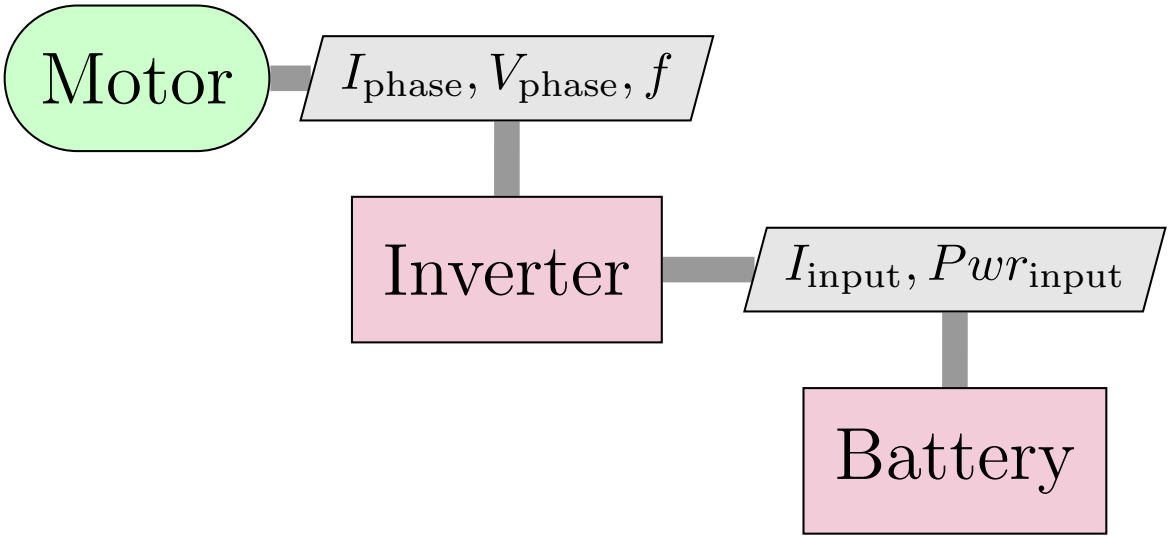

Figure 28: XDSM diagram for Drivetrain group

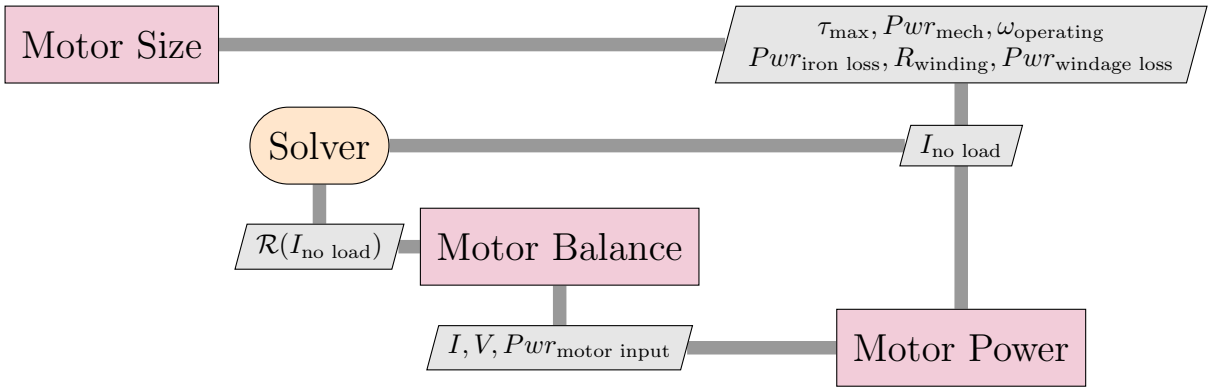

Figure 29: XDSM diagram for Motor group

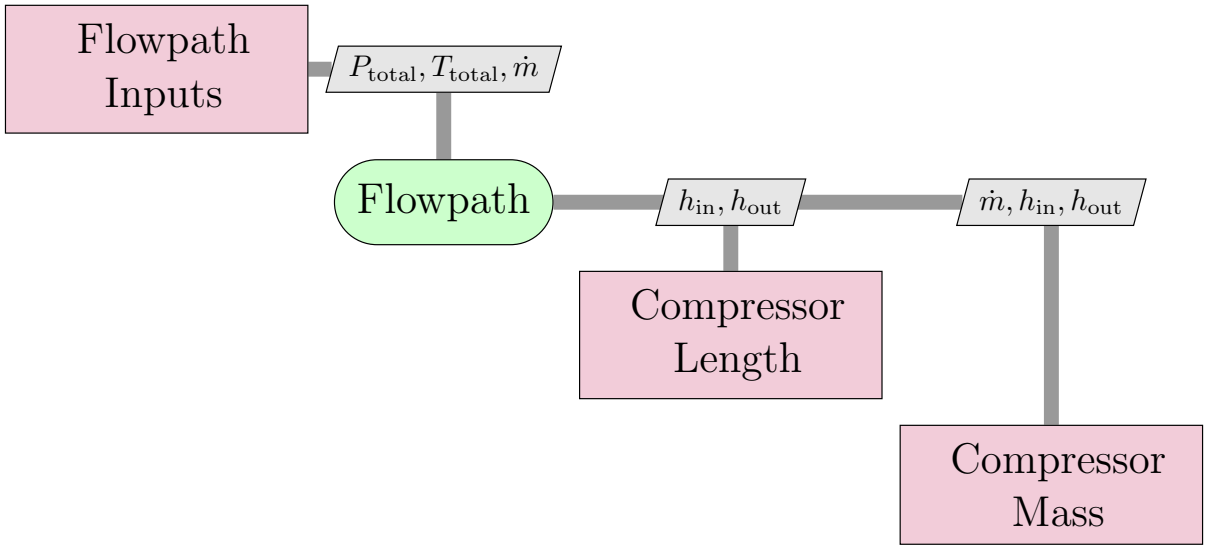

Figure 30: XDSM diagram for Cycle group

A. Drivetrain

1. Motor

1.1 MotorSize

1.2 MotorBalance

1.3 Motor

2. Inverter

3. Battery

B. PodGeometry

C. Cycle

1. Flowpath

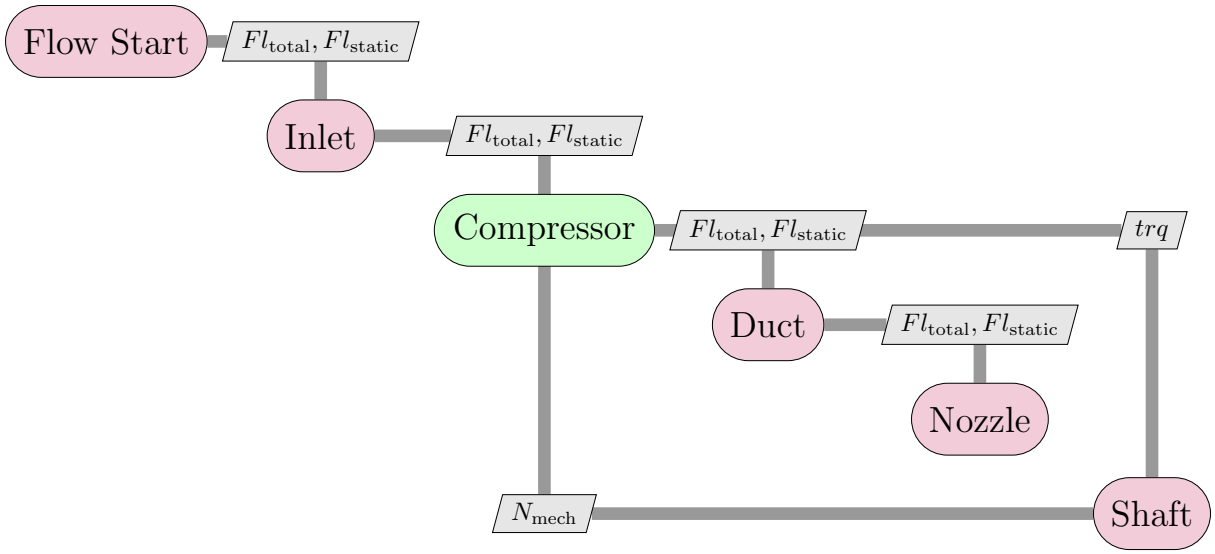

Figure 31: XDSM diagram for Flowpath group

1.1 CompressorLength

1.2 CompressorMass

1.3 FlowpathInputs

LevGroup

2. BreakpointDrag

3. MagneticDrag

4. MagneticMass

D. Drag

E. PodMach

F. PodMass

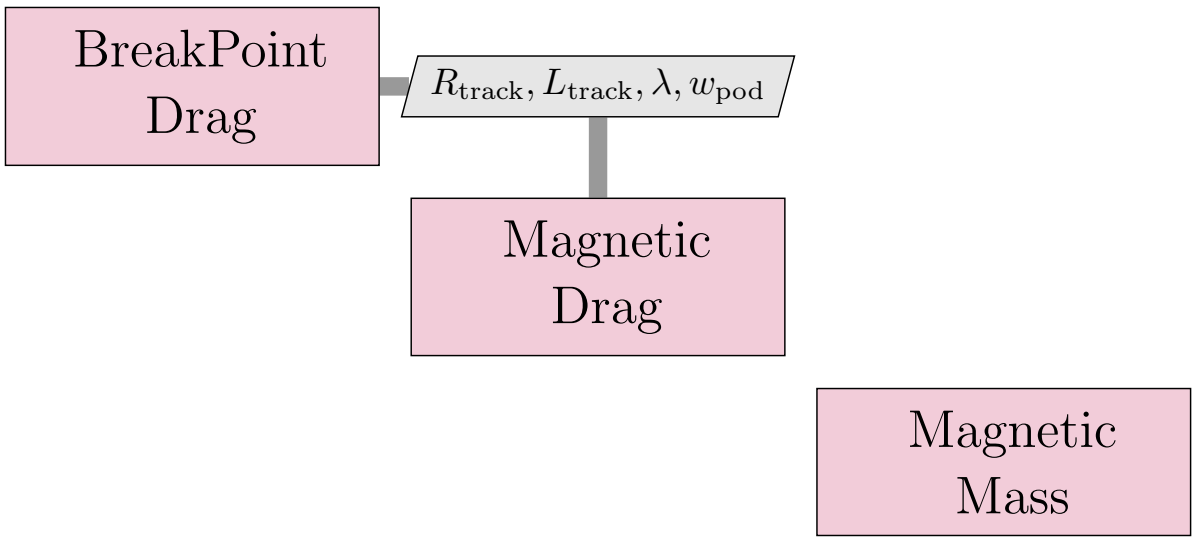

Figure 32: XDSM diagram for the LevGroup group

C. TicketCost

D. SampleMission

References

[1]Scott Jones Jeffrey Berton Jeffrey Chin, Justin Gray. Open-source conceptual sizing model of the hyperloop passenger pod. *AIAA Science and Technoloy Exposition*, 2014.

[2]Paul Friend. Magnetic levitation train technology 1. *progress report, Bradley university*, 2004.

[3]Elon Musk. Hyperloop alpha. Website, August 2013.

[4]Collins Gladin, Ali. Conceptual modeling of electric and hybrid-electric propulsion for uas applications. Sep 2015.

[5]Marty K Bradley and Christopher K Droney. Subsonic ultra green aircraft research. 2011.

[6]Justin Gray, Kenneth T. Moore, Tristan A. Hearn, and Bret A. Naylor. Standard platform for benchmarking multidisciplinary design analysis and optimization architectures. *AIAA Journal*, 51(10):2380–2394, Oct 2013.

[7]Eric Jones, Travis Oliphant, Pearu Peterson, et al. Scipy: Open source scientific tools for python, 2001. [Online; accessed 2016-09-26].